Revised Hamiltonian near third-integer resonance and implications for an electron storage ring

Ki Moon Nam,[1] Ji-Gwang Hwang,[2] Young Dae Yoon,[3,4,*] and Yong Woon Parc[5,1,†]

[1]*Division of Advanced Nuclear Engineering, Pohang University of Science and Technology, Pohang, Gyeongbuk 37673, Republic of Korea*
[2]*Gangneung-Wonju National University, Gangneung, Gangwon State 25457, Republic of Korea*
[3]*Asia Pacific Center for Theoretical Physics, Pohang, Gyeongbuk 37673, Republic of Korea*
[4]*Department of Physics, Pohang University of Science and Technology, Pohang, Gyeongbuk 37673, Republic of Korea*
[5]*Pohang Accelerator Laboratory, Pohang University of Science and Technology, Pohang, Gyeongbuk 37673, Republic of Korea*

(Received 17 May 2023; revised 11 January 2024; accepted 22 March 2024; published 18 April 2024)

In electron storage rings, an accurate description of particle dynamics near third-integer resonance is crucial for various applications. The conventional approach is to extrapolate far-resonance dynamics to near resonance, but the difficulty arises because the nonlinear detuning parameter diverges at this critical point. Here we derive, via a suitable application of the canonical perturbation theory, a revised detuning parameter that is well behaved near resonance. The resultant theory accurately describes the morphology of resonance islands for a wide range of parameter space and facilitates its optimization.

DOI: 10.1103/PhysRevAccelBeams.27.044001

I. INTRODUCTION

A charged particle in an electron storage ring experiences a periodic potential which makes the particle susceptible to various resonances. Such resonance phenomena have traditionally been viewed as detrimental to beam confinement, and operating the electron storage ring near resonance tunes has been avoided. However, if it has a certain nonlinear potential, it can form additional or secondary stable islands surrounding the central primary island. Various means are being revisited to actually utilize this resonance phenomenon in applications such as multi-turn extraction [1–4]. CERN has made significant progress in generating transverse resonance islands for proton beams across various resonance tune orders [1–4]. In this approach, the proton beam disperses from the main orbit to the secondary stable orbit for utilization, thereby avoiding the concurrent use of two orbits.

In operation modes of electron storage rings that utilize resonance islands, electrons are simultaneously confined to main and secondary stable orbits in transverse phase space [5]. Sextupole magnets in electron storage rings can form additional stable islands surrounding the central primary island. Previous research focus had been on eliminating these additional islands [6], but particles can actually be trapped in them by choosing the appropriate tune and applying external kicks [7], allowing for a multiobjective utilization of the stored beam [8,9]. This mode has been implemented at several facilities such as BESSY II [5] and MAX IV [10]. The presence of additional stable orbits in the ring has enabled pump-and-probe experiments with spatially separated short x-ray pulses [11], synchrotron-radiation-based electron time-of-flight spectroscopy [12], and control of x-ray helicity using APPLE-type undulators in conjunction with operation with resonance islands [9].

Despite the experimental implementation of resonance islands, the theoretical description of this phenomenon is still a subject of ongoing research and is not fully understood [13]. A widely used dynamical framework in electron storage ring physics is the Hamiltonian formalism [14–16]. When investigating higher-order effects beyond linear electron storage ring dynamics, a common approach is to separate long-term and short-term motions to derive an effective or average Hamiltonian that describes the system's long-term behavior and driving mechanisms. This mathematical approach has been applied to study amplitude-dependent tune shifts [17] and nonlinear chromaticity [18] in electron storage rings.

A key aspect for understanding resonance islands is the dynamical properties near the tune $\nu_x \cong l_{3\nu_x}/3$, which

*youngdae.yoon@apctp.org
†young1@postech.ac.kr

corresponds to the third-integer resonance. Near this resonance, the Hamiltonian has been proposed as [19]

$$\mathcal{H}(\phi,J)=\left(\nu_x-\frac{l_{3\nu_x}}{3}\right)J+g_{3,0,l_{3\nu_x}}J^{\frac{3}{2}}\cos(3\phi)+\frac{1}{2}\alpha_0 J^2, \tag{1}$$

where (ϕ,J) are the action-angle variables, ν_x is the horizontal tune, $l_{3\nu_x}$ is the integer number closest to $3\nu_x$, $g_{3,0,l_{3\nu_x}}$ is the resonance strength, and α_0 is the nonlinear detuning parameter [19,20]. In special cases like single kick approximation, Ω_2 is also used instead of α_0 [21]. However, α_0 diverges as $\nu_x\to\frac{l_{3\nu_x}}{3}$, and so this theory breaks down near the third-integer resonance around which resonance islands are supposed to form. In fact, in concurrent theoretical studies and applications of resonance islands, the detuning parameter is either deemed too difficult to derive [22] or just artificially supplemented or modified [13]. The derivation of the correct detuning parameter near resonance is therefore a crucial challenge in understanding and predicting resonance islands.

In this paper, we present a revised expression for the nonlinear detuning parameter using perturbative canonical transformations. The revised parameter is well behaved near third-integer resonance and so accurately describes the presence and morphology of the resonance islands. Particle tracking simulations using the lattice information of a currently operating electron storage ring (PLS-II) are performed and their results are shown to conform to the analytical predictions. The bearing of our findings on advanced operations of electron storage rings is discussed.

II. THEORY

A. Hamiltonian for a electron storage ring with sextupole magnet

The coordinate system (Frenet-Serret) employed in this study is depicted in Fig. 1. The Hamiltonian, as given in Eqs. (10)–(12) of Ref. [17], is presented below:

$$\mathcal{H}_1=\frac{I_x}{\beta_x(s)}+V(\phi_x,I_x,s), \tag{2}$$

$$V(\phi_x,I_x,s)=\frac{m(s)}{6\sqrt{2}}\left(\sqrt{\beta_x(s)I_x}\right)^3[\cos(3\phi_x)+3\cos(\phi_x)], \tag{3}$$

where $\beta_x(s)$ is a horizontal betatron function, (ϕ_x,I_x) is action-angle variables, and the sextupole magnet strength $m(s)$ is given by

$$m(s)=\frac{e}{p}\frac{\partial^2 B}{\partial x^2}. \tag{4}$$

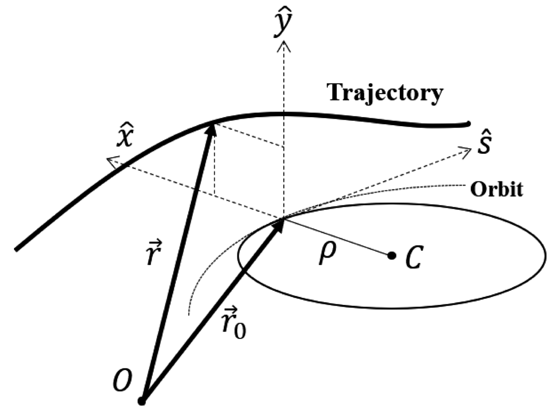

FIG. 1. The Frenet-Serret coordinate system used in this study. The particle moves along the trajectory line, with the position denoted by the vector $\vec{r}$. The origin of the Frenet-Serret coordinate system is denoted by the vector $\overrightarrow{r_0}$. The ideal orbit is represented by the dotted curved line. The bending radius is denoted by ρ, and the unit vectors of each axis are denoted by $\hat{x}$, $\hat{y}$, and $\hat{s}$.

In the above definitions, p is the momentum of an electron, e is the charge of an electron, and B is the magnetic field strength of the sextupole magnet.

A canonical transformation mapping from (ϕ_x,I_x) to (ψ_2,J_2) is performed using the second type of generating function, as given by [19]

$$F_2(\phi_x,J_2,s)=\left(\phi_x-\int_0^s\frac{1}{\beta_x(\tau)}d\tau+\frac{2\pi}{L}s\nu_x\right)J_2, \tag{5}$$

where L is the periodicity in the electron storage ring (for example, the length of a lattice or the circumference) and ν_x is defined as

$$\nu_x=\frac{1}{2\pi}\int_0^L\frac{1}{\beta_x(\tau)}d\tau. \tag{6}$$

Note that the 3 times of tune is near an integer, which is denoted as $3\nu_x\cong l_{3\nu_x}$. The new canonical action-angle variables are given below:

$$I_x=\frac{\partial F_2}{\partial\phi_x}=J_2, \tag{7}$$

$$\psi_2=\frac{\partial F_2}{\partial J_2}=\phi_x-\int_0^s\frac{1}{\beta_x(\tau)}d\tau+\frac{2\pi}{L}s\nu_x, \tag{8}$$

where the numerical subscript signifies the number of canonical transformations from the (x,x') position-momentum space. Replacing the system variable from s to $\theta=\frac{2\pi s}{L}=\frac{s}{R}$, the transformed Hamiltonian is given by

$$\mathcal{H}_2(\psi_2,J_2,\theta)=\nu_x J_2+V(\psi_2,J_2,\theta), \tag{9}$$

where

$$V(\psi_2, J_2, \theta) = \frac{Rm(\theta)}{6\sqrt{2}}\left[\left(\sqrt{\beta_x(\theta)J_2}\right)^3 \cos\left[3\psi_2 - 3\nu_x\theta + 3\chi_x(\theta)\right] + 3\left(\sqrt{\beta_x(\theta)J_2}\right)^3 \cos\left[\psi_2 - \nu_x\theta + \chi_x(\theta)\right]\right], \quad (10)$$

and

$$\chi_x(\theta) \equiv R\int_0^\theta \frac{1}{\beta_x(\Theta)} d\Theta. \quad (11)$$

Then, Fourier expanding V in θ, the Hamiltonian is now

$$\mathcal{H}_2(\psi_2, J_2, \theta) = \nu_x J_2 + \left(\sqrt{J_2}\right)^3 \sum_{n=-\infty}^{\infty} g_{3,0,n} \cos\left(3\psi_2 - n\theta + \xi_{3,0,n}\right) + \left(\sqrt{J_2}\right)^3 \sum_{n=-\infty}^{\infty} g_{1,0,n} \cos\left(\psi_2 - n\theta + \xi_{1,0,n}\right), \quad (12)$$

where the Fourier coefficients $g_{3,0,n}$, $\xi_{3,0,n}$, $g_{1,0,n}$, $\xi_{1,0,n}$ are given in Appendix A.

We now perform a canonical transformation using the generating function

$$G(\psi_2, J_3, \theta) = \left(\psi_2 - \frac{l_{3\nu_x}}{3}\theta\right)J_3, \quad (13)$$

which in effect eliminates the linear θ dependency of the angle variable. Then, the new Hamiltonian is given as

$$\begin{aligned}\mathcal{H}_3(\psi_3, J_3, \theta) &= \mathcal{H}_2(\psi_3, J_3, \theta) + \frac{\partial G(\psi_2, J_3, \theta)}{\partial\theta} \\ &= \delta_\nu J_3 + V(\psi_3, J_3, \theta),\end{aligned} \quad (14)$$

where the resonance proximity parameter δ_ν is defined by

$$\delta_\nu \equiv \nu_x - \frac{l_{3\nu_x}}{3} \quad (15)$$

and potential term is given by

$$V(\psi_3, J_3, \theta) = \left(\sqrt{J_3}\right)^3 \sum_{n=-\infty}^{\infty} g_{3,0,n} \cos\left(3\psi_3 + (l_{3\nu_x} - n)\theta + \xi_{3,0,n}\right) + \left(\sqrt{J_3}\right)^3 \sum_{n=-\infty}^{\infty} g_{1,0,n} \cos\left(\psi_3 + \left(\frac{l_{3\nu_x}}{3} - n\right)\theta + \xi_{1,0,n}\right). \quad (16)$$

While ψ_2 is a fast-varying variable, if $\frac{\partial V}{\partial J_3} \ll 1$, ψ_3 is now a slowly varying function of θ because $\frac{d\psi_3}{d\theta} = \frac{\partial\mathcal{H}_3}{\partial J_3} = \delta_\nu + \frac{\partial V}{\partial J_3} \ll 1$ near resonance. Then, Eq. (16) shows that V consists of fast-varying terms that depend on θ and a slowly varying term $\cos(3\psi_3 + \xi_{3,0,l_{3\nu_x}})$ which depends only on ψ_3.

B. Canonical perturbation and θ-independent Hamiltonian $\mathcal{H}_4$

Now we perform another perturbative canonical transformation from (ψ_3, J_3) to (ψ, J) that renders the transformed Hamiltonian to be explicitly θ-invariant for up to second order in $m(\theta)$ [17,23]. Consider a generating function, written in the following way:

$$F(\psi_3, J, \theta) = \psi_3 J + F^{(1)}(\psi_3, J, \theta) + F^{(2)}(\psi_3, J, \theta) + \cdots, \quad (17)$$

where $F^{(k)}$ denotes the kth order generating function. Here, the kth order means the proportionality to power of the function $m(\theta)$. The transformed action variable J is now determined by the following relation:

$$J_3 = \frac{\partial F(\psi_3, J, \theta)}{\partial\psi_3} = J + \frac{\partial F^{(1)}(\psi_3, J, \theta)}{\partial\psi_3} + \frac{\partial F^{(2)}(\psi_3, J, \theta)}{\partial\psi_3}. \quad (18)$$

The Hamiltonian $\mathcal{H}_4$ is given by

$$\mathcal{H}_4 = \mathcal{H}_3 + \frac{\partial F(\psi_3, J, \theta)}{\partial\theta}. \quad (19)$$

By using a Taylor series, the Hamiltonian $\mathcal{H}_4$ can be arranged in order of $m(\theta)$ and is given up to second order by

$$\mathcal{H}_4(\psi_3, J, \theta) \cong \mathcal{H}^{(0)} + \mathcal{H}^{(1)} + \mathcal{H}^{(2)}, \quad (20)$$

where

$$\mathcal{H}^{(0)} \equiv \delta_\nu J, \tag{21}$$

$$\mathcal{H}^{(1)} \equiv V(\psi_3, J, \theta) + \delta_\nu \frac{\partial F^{(1)}}{\partial \psi_3} + \frac{\partial F^{(1)}}{\partial \theta}, \tag{22}$$

$$\mathcal{H}^{(2)} \equiv \frac{\partial V(\psi_3, J, \theta)}{\partial J} \frac{\partial F^{(1)}}{\partial \psi_3} + \delta_\nu \frac{\partial F^{(2)}}{\partial \psi_3} + \frac{\partial F^{(2)}}{\partial \theta}. \tag{23}$$

Then $\mathcal{H}^{(n)}$ for $n \in \{0, 1, 2\}$ is θ invariant if the nth order generating function $F^{(n)}$ satisfies

$$\mathcal{H}^{(n)} - \langle \mathcal{H}^{(n)} \rangle_\theta = 0, \tag{24}$$

where $\langle A \rangle_\theta$ means the average of A over θ. Note that $\mathcal{H}^{(0)}$ is already θ invariant, so we start from $n = 1$.

For the first-order Hamiltonian $\mathcal{H}^{(1)}$, it should satisfy

$$\mathcal{H}^{(1)} - \langle \mathcal{H}^{(1)} \rangle_\theta = 0. \tag{25}$$

The θ average of the first-order Hamiltonian is given by

$$\begin{aligned}\langle \mathcal{H}^{(1)} \rangle_\theta &= \left\langle V(\psi_3, J, \theta) + \delta_\nu \frac{\partial F^{(1)}}{\partial \psi_3} + \frac{\partial F^{(1)}}{\partial \theta} \right\rangle_\theta \\ &= \langle V(\psi_3, J, \theta) \rangle_\theta + \delta_\nu \left\langle \frac{\partial F^{(1)}}{\partial \psi_3} \right\rangle_\theta + \left\langle \frac{\partial F^{(1)}}{\partial \theta} \right\rangle_\theta. \end{aligned} \tag{26}$$

All terms in $\langle V(\psi_3, J, \theta) \rangle_\theta$ are 0 except one term because other terms in $V(\psi_3, J, \theta)$ have explicit oscillatory dependency on θ. In order to satisfy $\mathcal{H}^{(1)} = \langle \mathcal{H}^{(1)} \rangle_\theta$, thus we need to find the generating function that satisfies the following relations:

$$\left\langle \frac{\partial F^{(1)}}{\partial \psi_3} \right\rangle_\theta = 0, \tag{27}$$

$$\left\langle \frac{\partial F^{(1)}}{\partial \theta} \right\rangle_\theta = 0. \tag{28}$$

Assuming that the above two equations are satisfied by some generating function, the first-order Hamiltonian is given by

$$\begin{aligned}\mathcal{H}^{(1)} &= \langle \mathcal{H}^{(1)} \rangle_\theta \\ &= \langle V(\psi_3, J, \theta) \rangle_\theta + \delta_\nu \left\langle \frac{\partial F^{(1)}}{\partial \psi_3} \right\rangle_\theta + \left\langle \frac{\partial F^{(1)}}{\partial \theta} \right\rangle_\theta \\ &= (\sqrt{J})^3 g_{3,0,l_{3\nu_x}} \cos\,(3\psi_3 + \xi_{3,0,l_{3\nu_x}}). \end{aligned} \tag{29}$$

From Eqs. (22) and (29), we can derive the following equation:

$$\left\{ \delta_\nu \frac{\partial}{\partial \psi_3} + \frac{\partial}{\partial \theta} \right\} F^{(1)} = -\left(V(\psi_3, J, \theta) - \left(\sqrt{J}\right)^3 g_{3,0,l_{3\nu_x}} \cos\,(3\psi_3 + \xi_{3,0,l_{3\nu_x}}) \right). \tag{30}$$

Using the above equation, we can determine the first-order generating function, $F^{(1)}(\psi_3, J, \theta)$. We try the following ansatz for the generating function based on the form of $V(\psi_3, J, \theta)$:

$$F^{(1)}(\psi_3, J, \theta) = J^{\frac{3}{2}} \sum_{n=-\infty, n \neq l_{3\nu_x}}^{\infty} f_{3,0,n} \sin\,(3\psi_3 - (n - l_{3\nu_x})\theta + \xi_{3,0,n}) + J^{\frac{3}{2}} \sum_{n=-\infty}^{\infty} f_{1,0,n} \sin\left(\psi_3 - \left(n - \frac{l_{3\nu_x}}{3}\right)\theta + \xi_{1,0,n}\right). \tag{31}$$

Note that the removed term $(n \neq l_{3\nu_x})$ is originated from fact that there is a missing term $g_{3,0,l_{3\nu_x}} J^{\frac{3}{2}} \cos(3\psi_3 + \xi_{3,0,l_{3\nu_x}})$ in the potential V at the right side of Eq. (30). We can obtain the following relations from Eqs. (30) and (31):

$$3\delta_\nu f_{3,0,n} + f_{3,0,n}\,(l_{3\nu_x} - n) = -g_{3,0,n}, \tag{32}$$

and

$$\delta_\nu f_{1,0,n} + f_{1,0,n} \left(\frac{l_{3\nu_x}}{3} - n \right) = -g_{1,0,n}. \tag{33}$$

Thus, using the definition of δ_ν, we obtain the coefficients of the first-order generating function as follows:

$$f_{a,0,n} = -\frac{g_{a,0,n}}{a\nu_x - n} \quad \text{for } a \in \{1, 3\}. \tag{34}$$

Now, we can calculate the second-order Hamiltonian using the following relation:

$$\mathcal{H}^{(2)} - \langle \mathcal{H}^{(2)} \rangle_\theta = 0. \tag{35}$$

The average value of the second-order Hamiltonian is calculated as follows:

$$\langle \mathcal{H}^{(2)} \rangle_\theta = \delta_\nu \left\langle \frac{\partial F^{(2)}}{\partial \psi_3} \right\rangle_\theta + \left\langle \frac{\partial F^{(2)}}{\partial \theta} \right\rangle_\theta + \left\langle \frac{\partial V(\psi_3, J, \theta)}{\partial J} \frac{\partial F^{(1)}}{\partial \psi_3} \right\rangle_\theta . \quad (36)$$

Following the same way as in the first-order Hamiltonian, we can assume the following:

$$\left\langle \frac{\partial F^{(2)}}{\partial \psi_3} \right\rangle_\theta = 0, \quad (37)$$

$$\left\langle \frac{\partial F^{(2)}}{\partial \theta} \right\rangle_\theta = 0. \quad (38)$$

Detailed discussion for the existence of $F^{(2)}(\psi_3, J, \theta)$ is given in Appendix B. Consequently, the second-order Hamiltonian contains only θ-invariant terms, which can be calculated to obtain the resulting expression:

$$\begin{aligned}
\langle \mathcal{H}^{(2)} \rangle_\theta &= \left\langle \frac{\partial V(\psi_3, J, \theta)}{\partial J} \frac{\partial F^{(1)}}{\partial \psi_3} \right\rangle_\theta \\
&= \frac{3}{4} J^2 \left\langle \sum_{n,n'=-\infty, n' \neq l_{3\nu_x}}^{\infty} 3 g_{3,0,n} f_{3,0,n'} \cos\left(-(n-n')\theta + \xi_{3,0,n} - \xi_{3,0,n'}\right) \right. \\
&\quad + \sum_{n,n'=-\infty}^{\infty} g_{1,0,n} f_{1,0,n'} \cos\left(-(n-n')\theta + \xi_{1,0,n} - \xi_{1,0,n'}\right) \\
&\quad \left. + \sum_{n,n'=-\infty, n \neq l_{3\nu_x}}^{\infty} 3 f_{3,0,n} g_{3,0,n'} \cos\left(6\psi_3 - (n+n'-2l_{3\nu_x})\theta + \xi_{3,0,n} + \xi_{3,0,n'}\right) \right\rangle_\theta \\
&= \frac{3}{4} J^2 \left\{ \sum_{n=-\infty, n \neq l_{3\nu_x}}^{\infty} 3 f_{3,0,n} g_{3,0,n} + \sum_{n=-\infty}^{\infty} f_{1,0,n} g_{1,0,n} \right. \\
&\quad \left. + \cos(6\psi_3) \sum_{n+n'=2l_{3\nu_x}, n \neq l_{3\nu_x}} 3 f_{3,0,n} g_{3,0,n'} \cos\xi_{3,0,n} \cos\xi_{3,0,n'} \right\} \\
&= \frac{1}{2} J^2 \left\{ \alpha_{-1} + \frac{3}{2} \cos(6\psi_3) \sum_{n+n'=2l_{3\nu_x}, n \neq l_{3\nu_x}} 3 f_{3,0,n} g_{3,0,n'} \cos\xi_{3,0,n} \cos\xi_{3,0,n'} \right\},
\end{aligned} \quad (39)$$

where

$$\alpha_{-1} = \frac{3}{2} \left(\sum_{n=-\infty, n \neq l_{3\nu_x}}^{\infty} 3 f_{3,0,n} g_{3,0,n} + \sum_{n=-\infty}^{\infty} f_{1,0,n} g_{1,0,n} \right). \quad (40)$$

For a mirror-symmetric ring, i.e., $m(\theta)$ and $\beta_x(\theta)$ are even functions of θ, the integrals in Eqs. (A12) and (A14) are both zero. This means that both $\xi_{3,0,n}$ and $\xi_{3,0,n'}$ are either 0 or π. Here we have assumed such a mirror-symmetric ring so that $\cos(A + \xi_{3,0,n} + \xi_{3,0,n'}) = \cos A \cos\xi_{3,0,n} \cos\xi_{3,0,n'}$ for any A. Note that for a nonmirror-symmetric ring, the theory can still be applied with appropriate changes to the cosine terms, albeit in a more complicated manner. The coefficient of $\cos(6\psi_3)$ can be expressed in the following form:

$$\begin{aligned}
\sum_{n+n'=2l_{3\nu_x}, n \neq l_{3\nu_x}} f_{3,0,n} g_{3,0,n'} \cos\xi_{3,0,n} \cos\xi_{3,0,n'} &= \sum_{k=-\infty, k \neq 0}^{\infty} \frac{g_{3,0,l_{3\nu_x}+k} g_{3,0,l_{3\nu_x}-k}}{k - 3\delta_\nu} \cos\xi_{3,0,l_{3\nu_x}+k} \cos\xi_{3,0,l_{3\nu_x}-k} \\
&\cong \sum_{k=-\infty, k \neq 0}^{\infty} \frac{g_{3,0,l_{3\nu_x}+k} g_{3,0,l_{3\nu_x}-k}}{k} \cos\xi_{3,0,l_{3\nu_x}+k} \cos\xi_{3,0,l_{3\nu_x}-k} + O(\delta_\nu).
\end{aligned} \quad (41)$$

In Eq. (41) because $n = l_{3\nu_x} - k$ and $n \neq l_{3\nu_x}$, we naturally have $k \neq 0$. The function under the summation in Eq. (41) is odd with respect to k, so the sum's lowest order value is zero, and Eq. (41) is $O(\delta_\nu)$. However, Eq. (40) is constant with respect to δ_ν, thus Eq. (41) can be disregarded (see details in Appendix C). Therefore, the second-order Hamiltonian can be obtained as follows:

$$\mathcal{H}^{(2)} = \frac{1}{2}\alpha_{-1}J^2. \tag{42}$$

The full Hamiltonian can be obtained from Eqs. (21), (29), and (42) as follows:

$$\mathcal{H}_4(\psi_3, J) \cong \delta_\nu J + g_{3,0,l_{3\nu_x}} J^{\frac{3}{2}} \cos\left(3\psi_3 + \xi_{3,0,l_{3\nu_x}}\right) + \frac{1}{2}\alpha_{-1}J^2. \tag{43}$$

To express the Hamiltonian in terms of new variables, we use the following relation between the old and new angle variables:

$$\psi \cong \psi_3 + \frac{\partial F^{(1)}(\psi_3, J, \theta)}{\partial J}, \tag{44}$$

where the last term $\Delta\psi$ is of first order in $m(\theta)$. However,

$$\begin{aligned} \cos\left(3\psi_3 + \xi_{3,0,l_{3\nu_x}}\right) &= \cos\left(3\psi + \xi_{3,0,l_{3\nu_x}} - \Delta\psi\right) \\ &= \cos(3\psi + \xi_{3,0,l_{3\nu_x}}) + O(\Delta\psi^2) \\ &\cong \cos(3\psi + \xi_{3,0,l_{3\nu_x}}). \end{aligned} \tag{45}$$

Here, the term $O(\Delta\psi^2)$ is removed because, being of second order in itself, it introduces a third-order effect in the Hamiltonian $\mathcal{H}_4$. Therefore, the resulting θ-invariant Hamiltonian $\mathcal{H}_4$ is obtained as follows:

$$\mathcal{H}_4(\psi, J) = \delta_\nu J + g_{3,0,l_{3\nu_x}} J^{\frac{3}{2}} \cos\left(3\psi + \xi_{3,0,l_{3\nu_x}}\right) + \frac{1}{2}\alpha_{-1}J^2. \tag{46}$$

It should be emphasized that the removed term in the summation in Eq. (40) corresponds to the slowly varying term in the first-order Hamiltonian in Eq. (22). By comparison to Eq. (1), we can express α_{-1} as the revised detuning parameter and it is one of our main results. The first (unperturbed), second (resonance driving), and third (detuning and island forming) terms in Eq. (46) correspond to $\mathcal{H}^{(0)}$, $\mathcal{H}^{(1)}$, and $\mathcal{H}^{(2)}$, respectively.

In contrast, the conventional detuning parameter in Eq. (1) is effectively given by

$$\alpha_0 = \frac{3}{2}\left(\sum_{n=-\infty}^{\infty} 3f_{3,0,n}g_{3,0,n} + \sum_{n=-\infty}^{\infty} f_{1,0,n}g_{1,0,n}\right). \tag{47}$$

The reason why Eq. (47) corresponds to Eq. (63) in Ref. [17] or Eq. (196) in Ref. [19] is given in Appendix D. Equation (47) is derived by averaging over both the faster-varying θ and the slowly varying ψ_3 in Eq. (24). The relation between Eq. (40) and (47) is given by

$$\alpha_0 = \alpha_{-1} + \frac{9}{2}\frac{{g_{3,0,l_{3\nu_x}}}^2}{l_{3\nu_x} - 3\nu_x}. \tag{48}$$

It is clear that the last term of Eq. (48), which is the removed term in Eq. (40), diverges when the tune ν_x is close to $l_{3\nu_x}/3$. Because of this removal, α_{-1} is well behaved and correctly describes near-resonance dynamics.

The analytical prediction given by α_{-1} will now be verified through comparisons to numerical simulations. An electron tracking code was written in MATLAB that treats dipole and quadrupole magnets as transfer matrices and solves sextupole effects using the fourth-order Runge-Kutta method. The algorithm was tested against the PLS-II electron storage ring lattice [24]. To facilitate the comparison, we define the following quantities:

$$X = \sqrt{J}\cos(\psi), \tag{49}$$

$$P = -\sqrt{J}\sin(\psi). \tag{50}$$

Note that above transform from (ψ, J) into (X, P) is also canonical.

Because $\xi_{3,0,l_{3\nu_x}}$ is 0 or π in mirror-symmetric ring (see Appendix A), Eq. (46) is now given by

$$\begin{aligned} \mathcal{H}_5(X,P) = {}& \delta_\nu\{X^2 + P^2\} + g_{3,0,l_{3\nu_x}}\cos(\xi_{3,0,l_{3\nu_x}})\{X^3 - 3XP^2\} \\ & + \frac{1}{2}\alpha_j\{X^2 + P^2\}^2, \end{aligned} \tag{51}$$

where $j = -1$ yields the revised detuning parameter in Eq. (40), and $j = 0$ yields the conventional detuning parameter in Eq. (47).

C. Size of secondary islands

In this part, we will show the relation between the size of secondary islands and the revised nonlinear parameter α_{-1}. Figure 2 exhibits an example of islands in phase space. We will calculate the fixed points of the islands on the horizontal axis ($P = 0$). According to the definition of fixed points, the fixed points must satisfy the following condition:

$$\begin{aligned} \frac{dP}{d\theta} &= \frac{\partial\mathcal{H}_5}{\partial X} \\ &= 2\delta_\nu X + 3\mathcal{G}(X^2 - P^2) + 2\alpha_{-1}(X^2 + P^2)X \\ &= 2\delta_\nu X + 3\mathcal{G}X^2 + 2\alpha_{-1}X^3 \\ &= 0, \end{aligned} \tag{52}$$

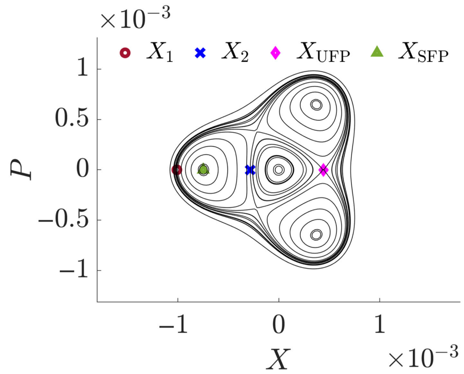

FIG. 2. Example of phase space configuration with $\mathcal{H}_5$.

where $\mathcal{G} = g_{3,0,l_{3\nu_x}} \cos \xi_{3,0,l_{3\nu_x}}$ to reduce notational clutter. The relation between the fixed points and α_{-1} is given by the following equation:

$$X_{\rm UFP} = \frac{-3\mathcal{G} + \sqrt{9\mathcal{G}^2 - 16\alpha_{-1}\delta_\nu}}{4\alpha_{-1}}. \tag{53}$$

$$X_{\rm SFP} = \frac{-3\mathcal{G} - \sqrt{9\mathcal{G}^2 - 16\alpha_{-1}\delta_\nu}}{4\alpha_{-1}}. \tag{54}$$

If $9\mathcal{G}^2 < 16\alpha_{-1}\delta_\nu$, secondary islands cannot be formed. As shown in Fig. 2, $X_{\rm UFP}$ lies at the apex of the central triangle while $X_{\rm SFP}$ is in the center of the island.

To describe the sizes of the island and the central triangle, the values of X_1 and X_2 in Fig. 2 need to be known. Since $\mathcal{H}_5(X,0) - \mathcal{H}_5(X_{\rm UFP},0)$ is a fourth-order polynomial with zero crossings at X_1, X_2, and $X_{\rm UFP}$, where $X_{\rm UFP}$ also corresponds to a local extrema, X_1 and X_2 should satisfy the next equation:

$$\begin{aligned}\mathcal{H}_5(X,0) &= \frac{\alpha_{-1}}{2}(X-X_{\rm UFP})^2(X-X_1)(X-X_2) + \mathcal{H}_5(X_{\rm UFP},0)\\ &= \delta_\nu X^2 + \mathcal{G}X^3 + \frac{1}{2}\alpha_{-1}X^4. \end{aligned}\tag{55}$$

By comparing the coefficients, we can compute X_1 and X_2 as follows:

$$X_1 = \frac{-\left(\mathcal{G} + \sqrt{9\mathcal{G}^2 - 16\alpha_{-1}\delta_\nu}\right) - \sqrt{4\mathcal{G}^2 + 4\mathcal{G}\sqrt{9\mathcal{G}^2 - 16\alpha_{-1}\delta_\nu}}}{4\alpha_{-1}}, \tag{56}$$

$$X_2 = \frac{-\left(\mathcal{G} + \sqrt{9\mathcal{G}^2 - 16\alpha_{-1}\delta_\nu}\right) + \sqrt{4\mathcal{G}^2 + 4\mathcal{G}\sqrt{9\mathcal{G}^2 - 16\alpha_{-1}\delta_\nu}}}{4\alpha_{-1}}. \tag{57}$$

III. NUMERICAL RESULTS

A. Validity of α_{-1}

While the designed tune of the PLS-II lattice is 1.273, the fiducial tune was set to 1.3325 to form resonance islands. There are four pairs of sextupole magnets (green boxes in Fig. 3) whose strengths determine the values of α_j. The behavior of α_j for the PLS-II lattice as a function of ν_x around the fiducial ν_x is presented in Fig. 4. The original detuning parameter α_0 (red line) diverges when the fractional tune is close to 1/3 (vertical dashed line) while the revised parameter α_{-1} (blue line) is well behaved near 1/3. At the fiducial tune $\nu_x = 1.3325$, α_0 is 2594.2 and α_{-1} is 1058.1 (circles in Fig. 4).

The simulated electron phase-space trajectories are shown as a Poincare section (red) in Fig. 5. About 10 electrons were initiated with $(X,P) = (X_0, 0)$, where X_0 uniformly ranges from −0.0017 to 0.0017 in normalized phase space. As they pass through the periodic lattice, their phase-space positions at the start of the lattice were recorded for 1500 cells. Also plotted in gray is a contour plot of Hamiltonian in Eq. (51) with α_{-1} [Fig. 5(a)] and α_0 [Fig. 5(b)]. There is good agreement between the Poincare section and the gray contour using α_{-1}. In contrast, the prediction given by α_0 does not conform to the simulation results.

To further contrast the analytical fidelity of α_{-1} to that of α_0, a parametric study was conducted by scanning the

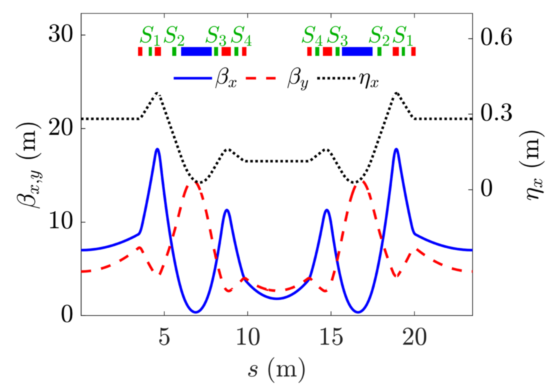

FIG. 3. The horizontal (blue) and vertical (red) beta functions, and the horizontal dispersion function (black) in PLS-II lattice. PLS-II is a “double bend achromat (DBA)” lattice. The initial horizontal beta function is $\beta_{x,0} = 7.006$ m and the tune is $\nu_x = 1.3325$. The rectangular inset illustrates the magnet distribution within PLS-II, where the red denotes the quadrupole magnets, the blue the bending magnets, and the green the sextupole magnets S_{1-4}.

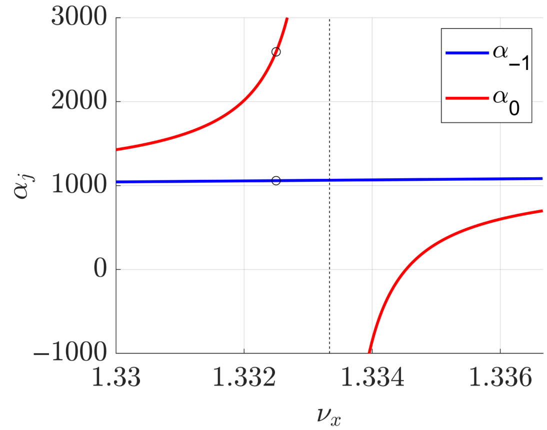

FIG. 4. Nonlinear detuning parameter vs tune. The original detuning parameter α_0 is plotted by red line. The revised detuning parameter α_{-1} is plotted by blue line. The circles denote the values of detuning parameters when the tune is $\nu_x = 1.3325$ for PLS-II lattice.

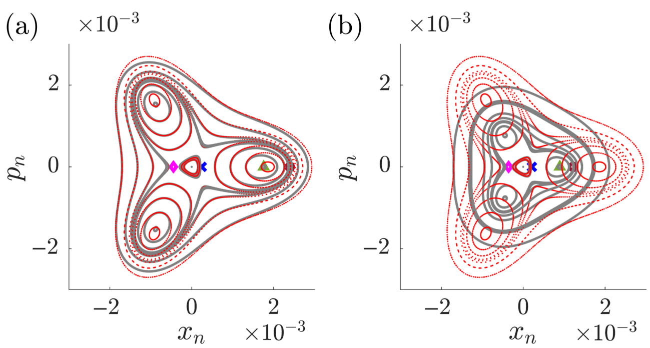

FIG. 5. (a) Phase-space trajectories with contour plots of the Hamiltonian in Eq. (51) where $\delta_\nu = -8.33 \times 10^{-4}$, $g_{3,0,l_{3\nu_x}} = -0.923$ and $j = -1$ (gray line). Red dots represent phase-space trajectories from tracking results. Normalized coordinates are defined as $(x_n = \frac{x}{\sqrt{2\beta_{x,0}}}, p_n = -\sqrt{\frac{\beta_{x,0}}{2}} x')$ where $\beta_{x,0}$ is the beta function at the starting position of the lattice. (b) Same as (a), but for $j = 0$.

strengths of the sextupoles S_{1-4}. Varying these strengths effectively changes the morphology of the Poincare section in Fig. 5. Then, the value of the detuning parameter that renders the contour to align exactly with the simulated Poincare section is dubbed α_1, i.e., α_1 is the empirical detuning parameter (see details in Appendix E). α_1 for different S_{1-4} are plotted in Fig. 6 (blue dots).

Also shown in Fig. 6 are α_{-1} (red lines) and α_0 (black dashed lines) as a function of the sextupole strengths. The dependency of α_{-1} and α_0 on S_{1-4} can be written as

$$\alpha_0(S_k) = a_{2,k} S_k^2 + 2a_{1,k} S_k + a_{0,k}, \tag{58}$$

$$\alpha_{-1}(S_k) = b_{2,k} S_k^2 + 2b_{1,k} S_k + b_{0,k}, \tag{59}$$

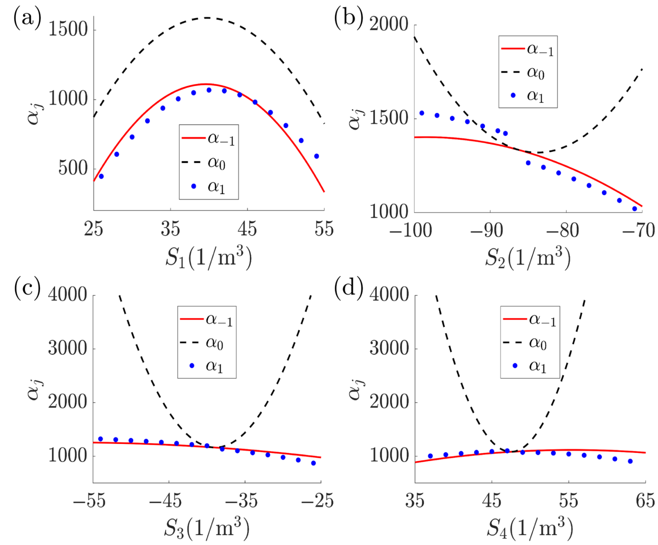

FIG. 6. The empirical nonlinear detuning parameter α_1 (blue dots) when (a) S_1, (b) S_2, (c) S_3, and (d) S_4 sextupole strength are varied. Also shown are α_{-1} (red lines) and α_0 (black dashed lines).

where $k \in \{1, 2, 3, 4\}$. These coefficients are derived in Appendix F. For instance in Fig. 6(c), the coefficients are calculated as $a_{2,3} = 17.887$ and $b_{2,3} = -0.251$. It is clear that α_{-1} agrees with α_1 better than α_0 does.

Another analytical prediction that the detuning parameter gives is the location of the fixed point of the rightmost island. The distance from the origin to the fixed point can be analytically derived from Eq. (51) and is given by [19],

$$\sqrt{J_{FP}} = \left| \frac{g_{3,0,l_{3\nu_x}}}{\alpha_j} \right| \left(\frac{3}{4} + \frac{3}{4} \sqrt{1 - \frac{16\alpha_j \delta_\nu}{9 g_{3,0,l_{3\nu_x}}^2}} \right). \tag{60}$$

The theoretical predictions of Eq. (60) with α_{-1} (red lines) and α_0 (black dashed lines) are plotted in Fig. 7. Again, the better agreement between α_{-1} and α_1 is clear.

In Fig. 7, there are regions in parameter space where α_{-1} and α_0 yield similar predictions (for example, around $S_3 = -40$ or $S_4 = 48$). This is because these are regions where $g_{3,0,l_{3\nu_x}}$ changes sign and therefore its magnitude becomes small. Then, at regions where $g_{3,0,l_{3\nu_x}} \ll \sqrt{\delta_\nu}$, $\alpha_{-1} \simeq \alpha_0$ by Eq. (48) and so the two detuning parameters are indistinguishable. This can actually be seen in Fig. 6 as well; the regions in question correspond to regions where $\alpha_{-1} \simeq \alpha_0$.

Figure 8 depicts the predicted fixed points using Eq. (60) while varying the tune. The red line represents the predictions using α_{-1} while the dashed black line represents the predictions using α_0. As the tune approaches 4/3, the predictions using α_0 exhibit larger errors. On the other hand, the predictions using α_{-1} show a better fit.

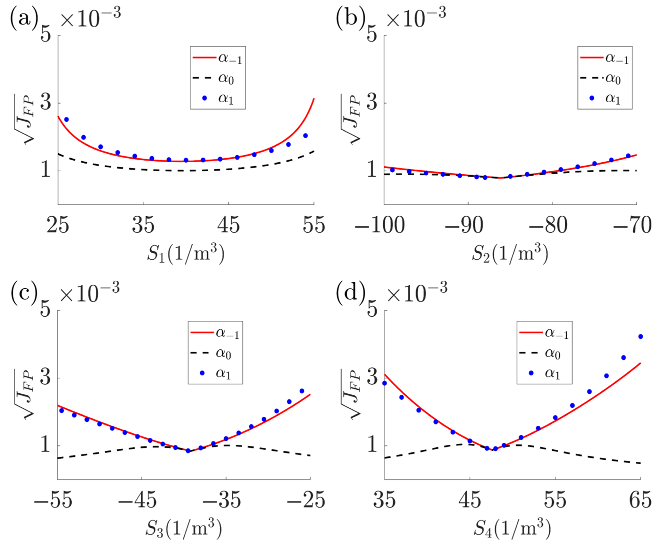

FIG. 7. Fixed points (blue dots) for varying (a) S_1, (b) S_2, (c) S_3, and (d) S_4. The theoretical prediction of Eq. (60) with α_{-1} is plotted in red solid line and that with α_0 is plotted in black dashed line.

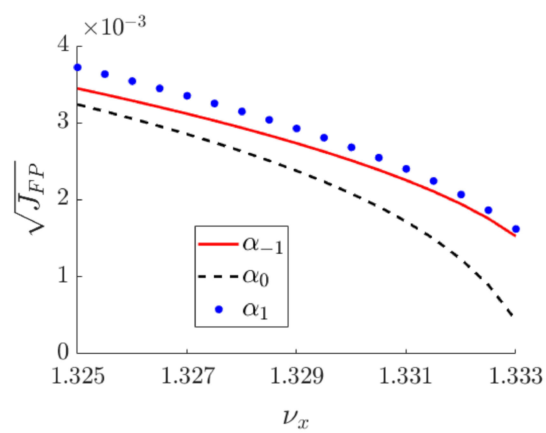

FIG. 8. Fixed points (blue dots) vs tune. The theoretical prediction of Eq. (60) with α_{-1} is plotted in red solid line and that with α_0 is plotted in black dashed line.

From the results presented in Figs. 6–8, we conclude that α_{-1} is a much better predictor of resonance islands in electron storage rings than α_0. It is also valid for a much wider range of sextupole strengths or when $g_{3,0,l_{3\nu_x}}$ is large. The simulation results shown so far are based on the lattice of PLS-II. However, because the only assumption behind the derivation of α_{-1} is that the tune is near the third-integer resonance, the theoretical result can be applied to any electron storage ring lattice. For instance, our predictions were also checked favorably against simulation results based on the BESSY-II lattice [25], which are not presented here.

There are still some discrepancies between the prediction by α_{-1} and the simulation results. These differences may come from higher order terms in the perturbation or from the approximations used in the derivation of the Hamiltonian in Eq. (46). As in the case of Ref. [17], the higher order terms can in principle be calculated and is left here for future work. Coupling with other motional degrees of freedom will also be left for future work, although for flat beams the present theory should suffice.

B. Optimization of secondary islands

In this section, a method is presented for optimizing the size of the secondary islands. Sextupoles in a electron storage ring can control not only the morphology of phase space but also chromaticities. The method introduced in this section allows for the adjustment of the size of secondary islands and center triangle while maintaining or changing both horizontal and vertical chromaticities to desired values.

From Eq. (55), we can derive next relations:

$$0 = X_{\mathrm{UFP}}(X_1 + X_2) + 2X_1X_2, \tag{61}$$

$$\frac{2\delta_\nu}{\alpha_{-1}} = X_{\mathrm{UFP}}^2 + 2X_{\mathrm{UFP}}(X_1 + X_2) + X_1X_2, \tag{62}$$

$$-\frac{2\mathcal{G}}{\alpha_{-1}} = 2X_{\mathrm{UFP}} + X_1 + X_2. \tag{63}$$

Because X_1 and X_2 determine the size of the secondary islands, one can choose the desired values of X_1 and X_2 and derive the required X_{UFP}, α_{-1}, and then $\mathcal{G}$ from Eqs. (61)–(63). Now what is left is to determine the sextupole strengths that yield these required values while maintaining particular desired chromaticities (ξ_x, ξ_y).

Because there are four target variables $(\alpha_{-1}, \mathcal{G}, \xi_x, \xi_y)$, there should be at least four pairs of sextupole magnets in one period. Now, S_1, S_2, and S_3 can be represented as follows:

$$\begin{pmatrix} S_1 \\ S_2 \\ S_3 \end{pmatrix} = \begin{pmatrix} \mu_1 & \mu_2 & \mu_3 \\ \zeta_{x,1} & \zeta_{x,2} & \zeta_{x,3} \\ \zeta_{y,1} & \zeta_{y,2} & \zeta_{y,3} \end{pmatrix}^{-1} \begin{pmatrix} \mathcal{G} - \mu_4 S_4 \\ \xi_x - \zeta_{x,4}S_4 \\ \xi_y - \zeta_{y,4}S_4 \end{pmatrix} \tag{64}$$

$$\equiv \begin{pmatrix} \kappa_1 - \sigma_1 S_4 \\ \kappa_2 - \sigma_2 S_4 \\ \kappa_3 - \sigma_3 S_4 \end{pmatrix}, \tag{65}$$

where $\mu_i = \partial\mathcal{G}/\partial S_i$, $\zeta_{x,i} = \partial\xi_x/\partial S_i$, and $\zeta_{y,i} = \partial\xi_y/\partial S_i$ for $i \in (1,2,3,4)$ [see Eqs. (F8), (F19), and (F20) for details]. Equation (64) effectively expresses S_{1-3} as linear functions of S_4. The coefficients κ_i and σ_i are functions of μ_i, $\zeta_{x,i}$, $\zeta_{y,i}$, $\mathcal{G}$, and $\xi_{x,y}$. Therefore, because $\alpha_{-1} = \sum_{i,j} \mathcal{A}_{ij} S_i S_j$ for

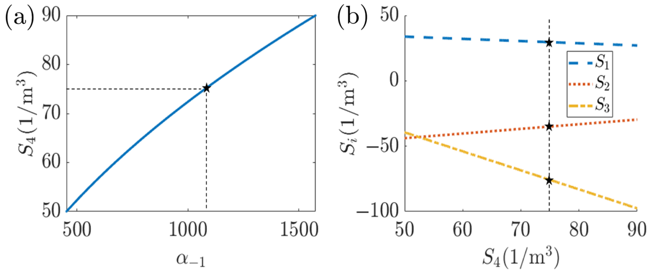

FIG. 9. (a) S_4 vs α_{-1}, (b) S_i ($i = 1, 2, 3$) vs S_4.

$i, j \in (1, 2, 3, 4)$ [see Eq. (F10)], α_{-1} can be expressed as a quadratic function of S_4 by using Eq. (65) as follows:

$$\alpha_{-1} = \left(\mathcal{A}_{44} - 2\sum_{i=1}^{3}\mathcal{A}_{4i}\sigma_i + \sum_{i,j=1}^{3}\mathcal{A}_{ij}\sigma_i\sigma_j\right)S_4^2 + 2\left(\sum_{i=1}^{3}\mathcal{A}_{4i}\kappa_i - \sum_{i,j=1}^{3}\mathcal{A}_{ij}\kappa_i\sigma_j\right)S_4 + \sum_{i,j=1}^{3}\mathcal{A}_{ij}\kappa_i\kappa_j \equiv \mathcal{B}_2 S_4^2 + 2\mathcal{B}_1 S_4 + \mathcal{B}_0. \tag{66}$$

Thus, knowing α_{-1}, one can obtain S_4 as follows:

$$S_4 = \frac{-\mathcal{B}_1 \pm \sqrt{\mathcal{B}_1^2 - \mathcal{B}_2(\mathcal{B}_0 - \alpha_{-1})}}{\mathcal{B}_2}. \tag{67}$$

For example, let us assume the desired boundaries are $X_1 = 2.39 \times 10^{-3}$ and $X_2 = 2.47 \times 10^{-4}$, and the desired chromaticities are $(\xi_x, \xi_y) = (3.016, 1.207)$. (X_1, X_2) can be converted to $(\alpha_{-1}, \mathcal{G})$ using Eqs. (61)–(63), which give $(\alpha_{-1}, \mathcal{G}) = (1058.1, -0.923)$. Now that the desired $(\alpha_{-1}, \mathcal{G}, \xi_x, \xi_y)$ are known, the above method can be used to first find S_4 from α_{-1} by using Eq. (67) [denoted as black star in Fig. 9(a)] and then find S_{1-3} from Eq. (65) [denoted as black stars in Fig. 9(b)]. The resulting set of sextupole strengths is $(S_1, S_2, S_3, S_4) = (29.67, -35.21, -74.84, 74.36)$. These are the parameters that were used in Fig. 5(a); the island boundaries indeed conform to the desired (X_1, X_2), and the chromaticities were also found to conform to the desired values.

IV. SUMMARY

In summary, we have derived a revised detuning parameter that is well behaved near third-integer resonance, in contradistinction to the conventional parameter that diverges near this critical point. The resultant Hamiltonian accurately predicts the morphology of resonance islands in transverse phase space, which are crucial for advanced electron storage ring operations. This new theory paves the way for the previously inaccessible, systematic optimization of island sizes and locations in phase space and reduces unnecessary efforts in haphazard empirical searches for secondary stable orbits.

ACKNOWLEDGMENTS

The authors would like to give special appreciation to Dr. K. Soutome in Japan Synchrotron Radiation Research Institute for his kind introduction for the Hamiltonian dynamics. The authors would like to appreciate to Dr. J. Y. Lee and Dr. Jaehyun Kim in PAL for their aid in the simulation in early stage of this study. The authors would like to thank Dr. P. Goslawski and Mr. M. Arlandoo in BESSY-II for the many helpful discussions. The authors would like to extend special thanks to Prof. A. Wolski for his fruitful advice for the theory. This work was supported National R&D Program (RS-2022-00154676) and partly by the Basic Science Research Program (2021R1F1A105123611) through the National Research Foundation of Korea (NRF) funded by the Ministry of Science and ICT. Y. D. Y. was supported by an appointment to the JRG Program at the APCTP through the Science and Technology Promotion Fund and Lottery Fund of the Korean Government and also by Korean local governments–Gyeongsangbuk-do province and Pohang city. Y. D. Y. was also supported by the POSCO Science Fellowship of POSCO TJ Park Foundation.

APPENDIX A: FOURIER EXPANSION OF SEXTUPOLE POTENTIAL

The sextupole potential in the Hamiltonian can be separated into two terms based on the coefficient of ψ_2 in the cosine function, as given by

$$V(\psi_2, J_2, \theta) = RV_1(\psi_2, J_2, \theta) + RV_2(\psi_2, J_2, \theta), \tag{A1}$$

where

$$V_1 = \left(\sqrt{J_2}\right)^3 \frac{m(\theta)}{6\sqrt{2}}\left(\sqrt{\beta_x(\theta)}\right)^3 \cos\left[3\psi_2 - 3\nu_x\theta + 3\chi_x(\theta)\right], \tag{A2}$$

$$V_2 = \left(\sqrt{J_2}\right)^3 \frac{m(\theta)}{2\sqrt{2}}\left(\sqrt{\beta_x(\theta)}\right)^3 \cos\left[\psi_2 - \nu_x\theta + \chi_x(\theta)\right]. \tag{A3}$$

We can separate the first subpotential V_1 as follows:

$$V_1 \equiv \left(\sqrt{J_2}\right)^3 M_{3,c}(\theta)\cos(3\psi_2) - \left(\sqrt{J_2}\right)^3 M_{3,s}(\theta)\sin(3\psi_2), \tag{A4}$$

where

$$M_{3,c}(\theta) \equiv \frac{m(\theta)}{6\sqrt{2}}\left(\sqrt{\beta_x(\theta)}\right)^3 \cos\left[-3\nu_x\theta + 3\chi_x(\theta)\right], \tag{A5}$$

$$M_{3,s}(\theta) \equiv \frac{m(\theta)}{6\sqrt{2}}\left(\sqrt{\beta_x(\theta)}\right)^3 \sin\left[-3\nu_x\theta + 3\chi_x(\theta)\right]. \tag{A6}$$

We can express the second subpotential V_2 in a similar manner as follows:

$$V_2 \equiv \left(\sqrt{J_2}\right)^3 M_{1,c}(\theta)\cos(\psi_2) - \left(\sqrt{J_2}\right)^3 M_{1,s}(\theta)\sin(\psi_2), \tag{A7}$$

where

$$M_{1,c}(\theta) \equiv \frac{m(\theta)}{2\sqrt{2}}\left(\sqrt{\beta_x(\theta)}\right)^3 \cos\left[-\nu_x\theta + \chi_x(\theta)\right], \tag{A8}$$

$$M_{1,s}(\theta) \equiv \frac{m(\theta)}{2\sqrt{2}}\left(\sqrt{\beta_x(\theta)}\right)^3 \sin\left[-\nu_x\theta + \chi_x(\theta)\right]. \tag{A9}$$

Equations (A5) and (A6) and (A8) and (A9), which are periodic functions of θ, contain all the θ dependency of the subpotentials V_1 and V_2, Note that V itself is not a periodic function of θ. Expressing the above functions by Fourier harmonics yields the following expression for the Hamiltonian:

$$\mathcal{H}_2(\psi_2, J_2, \theta) = \nu_x J_2 + \left(\sqrt{J_2}\right)^3 \sum_{n=-\infty}^{\infty} g_{3,0,n}\cos\left(3\psi_2 - n\theta + \xi_{3,0,n}\right) + \left(\sqrt{J_2}\right)^3 \sum_{n=-\infty}^{\infty} g_{1,0,n}\cos\left(\psi_2 - n\theta + \xi_{1,0,n}\right), \tag{A10}$$

where

$$g_{3,0,n}\cos\xi_{3,0,n} = \frac{R}{\pi}\int_0^{2\pi} \frac{m(\theta)}{12\sqrt{2}}\left(\sqrt{\beta_x(\theta)}\right)^3 \cos\left(-3\nu_x\theta + 3\chi_x(\theta) + n\theta\right)d\theta, \tag{A11}$$

$$g_{3,0,n}\sin\xi_{3,0,n} = \frac{R}{\pi}\int_0^{2\pi} \frac{m(\theta)}{12\sqrt{2}}\left(\sqrt{\beta_x(\theta)}\right)^3 \sin\left(-3\nu_x\theta + 3\chi_x(\theta) + n\theta\right)d\theta, \tag{A12}$$

$$g_{1,0,n}\cos\xi_{1,0,n} = \frac{R}{\pi}\int_0^{2\pi} \frac{m(\theta)}{4\sqrt{2}}\left(\sqrt{\beta_x(\theta)}\right)^3 \cos\left(-\nu_x\theta + \chi_x(\theta) + n\theta\right)d\theta, \tag{A13}$$

$$g_{1,0,n}\sin\xi_{1,0,n} = \frac{R}{\pi}\int_0^{2\pi} \frac{m(\theta)}{4\sqrt{2}}\left(\sqrt{\beta_x(\theta)}\right)^3 \sin\left(-\nu_x\theta + \chi_x(\theta) + n\theta\right)d\theta. \tag{A14}$$

If $m(\theta)$ and $\beta_x(\theta)$ are distributed mirror symmetrically, the oddness of the integrated function implies that Eqs. (A12) and (A14) are equal to zero. This implies that the Fourier expansion of sextupole potential have a phase of either zero or π. Another notable feature is that Eqs. (A11)–(A14) can be expressed in complex form as follows:

$$g_{3,0,n}e^{i\xi_{3,0,n}} = \frac{\sqrt{2}R}{24\pi}\int_0^{2\pi} m(\theta)\left(\sqrt{\beta_x(\theta)}\right)^3 \exp\left\{i\left[-(3\nu_x - n)\theta + 3\chi_x(\theta)\right]\right\}d\theta, \tag{A15}$$

$$g_{1,0,n}e^{i\xi_{1,0,n}} = \frac{\sqrt{2}R}{8\pi}\int_0^{2\pi} m(\theta)\left(\sqrt{\beta_x(\theta)}\right)^3 \exp\left\{i\left[-(\nu_x - n)\theta + \chi_x(\theta)\right]\right\}d\theta. \tag{A16}$$

APPENDIX B: DERIVATION OF THE SECOND-ORDER GENERATING FUNCTION $F^{(2)}(\psi_3, J, \theta)$

In this section, we derive the second-order generating function $F^{(2)}(\psi_3, J, \theta)$. In the context of a first-order generating function, we assumed that

$$\left\langle \frac{\partial F^{(1)}(\psi_3, J, \theta)}{\partial \psi_3} \right\rangle_\theta = \left\langle \frac{\partial F^{(1)}(\psi_3, J, \theta)}{\partial \theta} \right\rangle_\theta = 0 \tag{B1}$$

and derived $F^{(1)}(\psi_3, J, \theta)$ using Eq. (25). Subsequently, we showed that both $\langle \frac{\partial F^{(1)}(\psi_3, J, \theta)}{\partial \psi_3} \rangle_\theta$ and $\langle \frac{\partial F^{(1)}(\psi_3, J, \theta)}{\partial \theta} \rangle_\theta$ are actually zero. Applying the same logic, for the second-order generating function $F^{(2)}(\psi_3, J, \theta)$, we now assume that

$$\left\langle \frac{\partial F^{(2)}(\psi_3, J, \theta)}{\partial \psi_3} \right\rangle_\theta = \left\langle \frac{\partial F^{(2)}(\psi_3, J, \theta)}{\partial \theta} \right\rangle_\theta = 0. \tag{B2}$$

After this assumption, if we find the second-order generating function using Eq. (35) and if this function satisfies the above condition, the aforementioned assumption holds true. The differential equation for second-order generating function is given as follows:

$$\delta_\nu \frac{\partial F^{(2)}}{\partial \psi_3} + \frac{\partial F^{(2)}}{\partial \theta} = -\frac{\partial F^{(1)}}{\partial \psi_3}\frac{\partial V}{\partial J} + \frac{1}{2}\alpha_{-1}J^2. \tag{B3}$$

First-order generating function is given as follows:

$$F^{(1)}(\psi_3,J,\theta)=J^{\frac{3}{2}}\sum_{n=-\infty,n\neq l_{3\nu x}}^{\infty}f_{3,0,n}\sin(3\psi_3-(n-l_{3\nu_x})\theta+\xi_{3,0,n})+J^{\frac{3}{2}}\sum_{n=-\infty}^{\infty}f_{1,0,n}\sin\left(\psi_3-\left(n-\frac{l_{3\nu_x}}{3}\right)\theta+\xi_{1,0,n}\right). \quad \text{(B4)}$$

For simplicity, if we set $f_{3,0,l_{3\nu_x}}=0$ only for notational reasons, above equation can be simplified as follows:

$$\begin{aligned}F^{(1)}(\psi_3,J,\theta)&=J^{\frac{3}{2}}\sum_{n=-\infty,n\neq l_{3\nu x}}^{\infty}f_{3,0,n}\sin\left(3\psi_3-(n-l_{3\nu_x})\theta+\xi_{3,0,n}\right)+J^{\frac{3}{2}}\sum_{n=-\infty}^{\infty}f_{1,0,n}\sin\left(\psi_3-\left(n-\frac{l_{3\nu_x}}{3}\right)\theta+\xi_{1,0,n}\right)\\&=\sum_{a\in(1,3)}\sum_{n=-\infty}^{\infty}f_{a,0,n}\sin\left(a\psi_3-\left(n-\frac{a}{3}l_{3\nu_x}\right)\theta+\xi_{a,0,n}\right).\end{aligned} \quad \text{(B5)}$$

With same notation, V can be denoted as follows:

$$\begin{aligned}V(\psi_3,J,\theta)&=J^{\frac{3}{2}}\sum_{n=-\infty}^{\infty}g_{3,0,n}\cos\left(3\psi_3+(l_{3\nu_x}-n)\theta+\xi_{3,0,n}\right)+J^{\frac{3}{2}}\sum_{n=-\infty}^{\infty}g_{1,0,n}\cos\left(\psi_3+\left(\frac{l_{3\nu_x}}{3}-n\right)\theta+\xi_{1,0,n}\right)\\&=\sum_{a\in(1,3)}\sum_{n=-\infty}^{\infty}g_{a,0,n}\cos\left(a\psi_3-\left(n-\frac{a}{3}l_{3\nu_x}\right)\theta+\xi_{a,0,n}\right).\end{aligned} \quad \text{(B6)}$$

To estimate the form of second-order generating function, by expanding $\frac{\partial V}{\partial J}\frac{\partial F^{(1)}}{\partial\psi_3}$, we can obtain the following relations:

$$\begin{aligned}\frac{\partial F^{(1)}}{\partial\psi_3}\frac{\partial V}{\partial J}&=\frac{3}{2}J^2\left(\sum_{a\in(1,3)}\sum_{n=-\infty}^{\infty}af_{a,0,n}\cos\left(a\psi_3-\left(n-\frac{a}{3}l_{3\nu_x}\right)\theta+\xi_{a,0,n}\right)\right)\\&\quad\times\left(\sum_{a\in(1,3)}\sum_{n=-\infty}^{\infty}g_{a,0,n}\cos\left(a\psi_3-\left(n-\frac{a}{3}l_{3\nu_x}\right)\theta+\xi_{a,0,n}\right)\right)\\&=\frac{3}{2}J^2\sum_{a,b\in(1,3)}\sum_{n,r=-\infty}^{\infty}bg_{a,0,r}f_{b,0,n}\cos\left(a\psi_3-\left(n-\frac{a}{3}l_{3\nu_x}\right)\theta+\xi_{a,0,n}\right)\cos\left(b\psi_3-\left(r-\frac{b}{3}l_{3\nu_x}\right)\theta+\xi_{b,0,r}\right)\\&=\frac{3}{4}J^2\sum_{a\in(1,3)}\sum_{b\in(-3,-1,1,3)}\sum_{n,r=-\infty}^{\infty}\Big[|b|g_{a,0,r}f_{|b|,0,n}\\&\quad\times\cos\left((a+b)\psi_3+\frac{1}{3}(a+b)l_{3\nu}\theta-(r+sgn(b)n)\frac{s}{R}+\xi_{a,0,r}+sgn(b)\xi_{|b|,0,n}\right)\Big].\end{aligned} \quad \text{(B7)}$$

We can try the following ansatz for the second-order generating function based on the form of $\frac{\partial F^{(1)}}{\partial\psi_3}\frac{\partial V}{\partial J}$ as follows:

$$\begin{aligned}F^{(2)}(\psi_3,J,\theta)=J^2&\sum_{a\in(1,3)}\sum_{b\in(-3,-1,1,3)}\sum_{n,r=-\infty}^{\infty}\Big[f_{a,b,r,n}\\&\times\sin\left((a+b)\psi_3+\frac{1}{3}(a+b)l_{3\nu}\theta-(r+sgn(b)n)\frac{s}{R}+\xi_{a,0,r}+sgn(b)\xi_{|b|,0,n}\right)\Big].\end{aligned} \quad \text{(B8)}$$

This satisfies following equation:

$$\delta_\nu \frac{\partial F^{(2)}}{\partial \psi_3} + \frac{\partial F^{(2)}}{\partial \theta} = \frac{1}{2}\alpha_{-1}J^2 - \frac{3}{4}J^2 \sum_{a\in(1,3)} \sum_{b\in(-3,-1,1,3)} \sum_{n,r=-\infty}^{\infty} \Bigg[|b| g_{a,0,r} f_{|b|,0,n} \times \cos\left((a+b)\psi_3 + \frac{1}{3}(a+b) l_{3\nu}\theta - (r + sgn(b)n)\frac{s}{R} + \xi_{a,0,r} + sgn(b)\xi_{|b|,0,n} \right) \Bigg]. \tag{B9}$$

From definition of α_{-1},

$$\alpha_{-1} = \frac{3}{2} \sum_{a+b=0, a\in(3,1)} \sum_{n,r=-\infty}^{\infty} \Bigg[|b| g_{a,0,r} f_{|b|,0,n} \cos\left((a+b)\psi_3 + \frac{1}{3}(a+b) l_{3\nu}\theta - (r + sgn(b)n)\frac{s}{R} + \xi_{a,0,r} + sgn(b)\xi_{|b|,0,n} \right) \Bigg]. \tag{B10}$$

Thus, the cases where $a + b = 0$ and $r + sgn(b)n = 0$ are removed due to α_{-1}. In this case,

$$f_{a,-a,n,n} = 0. \tag{B11}$$

In other instances, the coefficient of second-order generating function is expressed as

$$f_{a,b,r,n} = \frac{-\frac{3|b|}{4} g_{a,0,r} f_{|b|,0,n}}{\delta_\nu(a+b) + (a+b)\frac{l_{3\nu}}{3} - (r + sgn(b)n)} = \frac{-\frac{3|b|}{4} g_{a,0,r} f_{|b|,0,n}}{(a+b)\nu_x - (r + sgn(b)n)}. \tag{B12}$$

Since $f_{a,-a,n,n} = 0$, it always has a term periodic in θ and thus indeed,

$$\left\langle \frac{\partial F^{(2)}(\psi_3, J, \theta)}{\partial \psi_3} \right\rangle_\theta = \left\langle \frac{\partial F^{(2)}(\psi_3, J, \theta)}{\partial \theta} \right\rangle_\theta = 0. \tag{B13}$$

APPENDIX C: δ_ν DEPENDENCE OF THE SECOND-ORDER COEFFICIENTS

In this section, we describe the physical properties of the α_{-1}, α_0, and α_6 with respect to δ_ν. Here, α_6 represents the coefficient of $\cos 6\psi_3$. The definitions of these parameters are given as follows:

$$\begin{aligned} \alpha_{-1} &= \frac{9}{2} \sum_{n=-\infty, n\neq l_{3\nu_x}}^{\infty} g_{3,0,n} f_{3,0,n} + \frac{3}{2} \sum_{n=-\infty}^{\infty} g_{1,0,n} f_{1,0,n}, \\ \alpha_0 &= \frac{9}{2} \sum_{n=-\infty}^{\infty} g_{3,0,n} f_{3,0,n} + \frac{3}{2} \sum_{n=-\infty}^{\infty} g_{1,0,n} f_{1,0,n}, \\ \alpha_6 &= \frac{9}{2} \sum_{n+n'=2l_{3\nu_x}, n\neq= l_{3\nu_x}} f_{3,0,n} g_{3,0,n'} \cos\xi_{3,0,n} \cos\xi_{3,0,n'}, \end{aligned} \tag{C1}$$

where $g_{3,0,n}$ and $g_{1,0,n}$ are Fourier coefficients defined by Eqs. (A11)–(A14), and $f_{3,0,n}$ and $f_{1,0,n}$ are first-order generating functions defined by Eq. (34). These parameters can be represented as power series in terms of δ_ν. The coefficients of these power series effectively represent the physical characteristics of each parameter. To simplify the argument, we assume that there is no dependence of $g_{3,0,n}$ and $g_{1,0,n}$ on δ_ν. Under this assumption, α_{-1} is expanded as follows:

$$\begin{aligned} \alpha_{-1} &= \frac{9}{2} \sum_{n=-\infty, n\neq l_{3\nu_x}}^{\infty} g_{3,0,n} f_{3,0,n} + \frac{3}{2} \sum_{n=-\infty}^{\infty} g_{1,0,n} f_{1,0,n}, \\ &= \frac{9}{2} \sum_{n=-\infty, n\neq l_{3\nu_x}}^{\infty} \frac{g_{3,0,n}^2}{n - 3\nu_x} + \frac{3}{2} \sum_{n=-\infty}^{\infty} \frac{g_{1,0,n}^2}{n - \nu_x} \\ &= \frac{9}{2} \sum_{k=-\infty, k\neq 0}^{\infty} \frac{g_{3,0,k+l_{3\nu_x}}^2}{k - 3\delta_\nu} + \frac{3}{2} \sum_{n=-\infty}^{\infty} \frac{g_{1,0,n}^2}{\left(n - \frac{l_{3\nu_x}}{3}\right) - \delta_\nu} \end{aligned}$$

$$
\begin{aligned}
&= \left(\frac{9}{2}\sum_{k=-\infty,k\neq 0}^{\infty}\frac{g^2_{3,0,k+l_{3\nu_x}}}{k} + \frac{3}{2}\sum_{n=-\infty}^{\infty}\frac{g^2_{1,0,n}}{\left(n-\frac{l_{3\nu_x}}{3}\right)}\right) + \left(\frac{27}{2}\sum_{k=-\infty,k\neq 0}^{\infty}\frac{g^2_{3,0,k+l_{3\nu_x}}}{k^2} + \frac{3}{2}\sum_{n=-\infty}^{\infty}\frac{g^2_{1,0,n}}{\left(n-\frac{l_{3\nu_x}}{3}\right)^2}\right)\delta_\nu \\
&\quad + \left(\frac{81}{2}\sum_{k=-\infty,k\neq 0}^{\infty}\frac{g^2_{3,0,k+l_{3\nu_x}}}{k^3} + \frac{3}{2}\sum_{n=-\infty}^{\infty}\frac{g^2_{1,0,n}}{\left(n-\frac{l_{3\nu_x}}{3}\right)^3}\right)\delta_\nu^2 + \cdots \\
&\equiv \alpha_{-1,0} + \alpha_{-1,1}\delta_\nu + \alpha_{-1,2}\delta_\nu^2 + \cdots, \qquad \text{(C2)}
\end{aligned}
$$

where we used the formula $\frac{1}{1-x} = \sum_{n=0}^{\infty} x^n (|x| < 1)$. α_0 can be expanded using the same procedure except that the term $-\frac{3g^2_{3,0,l_{3\nu_x}}}{2\delta_\nu}$ can be omitted, and it is expressed as follows:

$$
\begin{aligned}
\alpha_0 &= \frac{9}{2}\sum_{n=-\infty}^{\infty} g_{3,0,n} f_{3,0,n} + \frac{3}{2}\sum_{n=-\infty}^{\infty} g_{1,0,n} f_{1,0,n}, \\
&= \frac{9}{2}\sum_{n=-\infty}^{\infty}\frac{g^2_{3,0,n}}{n-3\nu_x} + \frac{3}{2}\sum_{n=-\infty}^{\infty}\frac{g^2_{1,0,n}}{n-\nu_x} \\
&= -\frac{3g^2_{3,0,l_{3\nu_x}}}{2\delta_\nu} + \frac{9}{2}\sum_{k=-\infty,k\neq 0}^{\infty}\frac{g^2_{3,0,k+l_{3\nu_x}}}{k-3\delta_\nu} + \frac{3}{2}\sum_{n=-\infty}^{\infty}\frac{g^2_{1,0,n}}{\left(n-\frac{l_{3\nu_x}}{3}\right)-\delta_\nu} \\
&= -\frac{3g^2_{3,0,l_{3\nu_x}}}{2\delta_\nu} + \left(\frac{9}{2}\sum_{k=-\infty,k\neq 0}^{\infty}\frac{g^2_{3,0,k+l_{3\nu_x}}}{k} + \frac{3}{2}\sum_{n=-\infty}^{\infty}\frac{g^2_{1,0,n}}{\left(n-\frac{l_{3\nu_x}}{3}\right)}\right) + \left(\frac{27}{2}\sum_{k=-\infty,k\neq 0}^{\infty}\frac{g^2_{3,0,k+l_{3\nu_x}}}{k^2} + \frac{3}{2}\sum_{n=-\infty}^{\infty}\frac{g^2_{1,0,n}}{\left(n-\frac{l_{3\nu_x}}{3}\right)^2}\right)\delta_\nu \\
&\quad + \left(\frac{81}{2}\sum_{k=-\infty,k\neq 0}^{\infty}\frac{g^2_{3,0,k+l_{3\nu_x}}}{k^3} + \frac{3}{2}\sum_{n=-\infty}^{\infty}\frac{g^2_{1,0,n}}{\left(n-\frac{l_{3\nu_x}}{3}\right)^3}\right)\delta_\nu^2 + \cdots \\
&\equiv \frac{\alpha_{0,-1}}{\delta_\nu} + \alpha_{0,0} + \alpha_{0,1}\delta_\nu + \alpha_{0,2}\delta_\nu^2 + \cdots. \qquad \text{(C3)}
\end{aligned}
$$

α_6 is given as follows:

$$
\begin{aligned}
\alpha_6 &= \frac{9}{2}\sum_{n+n'=2l_{3\nu_x},n\neq=l_{3\nu_x}} f_{3,0,n} g_{3,0,n'} \cos\xi_{3,0,n}\cos\xi_{3,0,n'} \\
&= \frac{9}{2}\sum_{k=-\infty,k\neq 0}^{\infty}\frac{g_{3,0,l_{3\nu_x}-k}\,g_{3,0,l_{3\nu_x}+k}}{k-3\delta_\nu}\cos\xi_{3,0,l_{3\nu_x}+k}\cos\xi_{3,0,l_{3\nu_x}-k} \\
&= \frac{9}{2}\sum_{k=-\infty,k\neq 0}^{\infty}\frac{g_{3,0,l_{3\nu_x}-k}\,g_{3,0,l_{3\nu_x}+k}}{k}\cos\xi_{3,0,l_{3\nu_x}+k}\cos\xi_{3,0,l_{3\nu_x}-k} + \frac{27}{2}\delta_\nu\sum_{k=-\infty,k\neq 0}^{\infty}\frac{g_{3,0,l_{3\nu_x}-k}\,g_{3,0,l_{3\nu_x}+k}}{k^2}\cos\xi_{3,0,l_{3\nu_x}+k}\cos\xi_{3,0,l_{3\nu_x}-k} \\
&\quad + \frac{81}{2}{\delta_\nu}^2\sum_{k=-\infty,k\neq 0}^{\infty}\frac{g_{3,0,l_{3\nu_x}-k}\,g_{3,0,l_{3\nu_x}+k}}{k^3}\cos\xi_{3,0,l_{3\nu_x}+k}\cos\xi_{3,0,l_{3\nu_x}-k} + \cdots. \\
&\equiv \alpha_{6,0} + \alpha_{6,1}\delta_\nu + \alpha_{6,2}\delta_\nu^2 + \cdots. \qquad \text{(C4)}
\end{aligned}
$$

Considering the coefficients of the $2p$th power of δ_ν (p is non-negative integer), denoted as $\alpha_{6,2p}$, these coefficients are given as summations of $g_{3,0,l_{3\nu_x}-k}\,g_{3,0,l_{3\nu_x}+k}\cos\xi_{l_{3\nu_x}+k}\cos\xi_{l_{3\nu_x}-k}$ divided by the $2p+1$th power of k. The value of $\alpha_{6,2p}$ is calculated as follows:

$$\begin{aligned}\alpha_{6,2p} &= \sum_{k=-\infty,k\neq 0}^{\infty} \frac{g_{3,0,l_{3\nu_x}-k}g_{3,0,l_{3\nu_x}+k}}{k^{2p+1}} \cos\xi_{l_{3\nu_x}+k}\cos\xi_{l_{3\nu_x}-k} \\ &= \sum_{k=-\infty}^{-1} \frac{g_{3,0,l_{3\nu_x}-k}g_{3,0,l_{3\nu_x}+k}}{k^{2p+1}} \cos\xi_{l_{3\nu_x}+k}\cos\xi_{l_{3\nu_x}-k} + \sum_{k=1}^{\infty} \frac{g_{3,0,l_{3\nu_x}-k}g_{3,0,l_{3\nu_x}+k}}{k^{2p+1}} \cos\xi_{l_{3\nu_x}+k}\cos\xi_{l_{3\nu_x}-k} \\ &= -\sum_{k=1}^{\infty} \frac{g_{3,0,l_{3\nu_x}+k}g_{3,0,l_{3\nu_x}-k}}{k^{2p+1}} \cos\xi_{l_{3\nu_x}-k}\cos\xi_{l_{3\nu_x}+k} + \sum_{k=1}^{\infty} \frac{g_{3,0,l_{3\nu_x}-k}g_{3,0,l_{3\nu_x}+k}}{k^{2p+1}} \cos\xi_{l_{3\nu_x}+k}\cos\xi_{l_{3\nu_x}-k} \\ &= 0. \end{aligned} \tag{C5}$$

This derivation demonstrates that the summands in the even powers of δ_ν are always zero and so only odd powers of δ_ν remain. Therefore, α_6 can be expressed as follows:

$$\alpha_6 = \alpha_{6,1}\delta_\nu + \alpha_{6,3}\delta_\nu^3 + \cdots. \tag{C6}$$

We can see that while α_0 and α_{-1} have terms that are bigger than $O(\delta_\nu)$, α_6 is only of $O(\delta_\nu)$. Therefore, $\alpha_6 \ll \alpha_0, \alpha_{-1}$.

Figure 10 shows the graph of Eq. (C1) in 10(a) and compares the fitting results up to the first order of δ_ν with each parameter α_{-1} [Fig. 10(b)], α_0 [Fig. 10(c)], and α_6 [Fig. 10(d)]. In Fig. 10(b), the results of fitting α_{-1} to δ_ν are $\alpha_{-1,1} = 6056$, $\alpha_{-1,0} = 1063$, and $\alpha_{-1,-1} = 0$. It describes that α_{-1} does not exhibit a term that diverges at $\nu_x = \frac{4}{3}$. In case of α_0 shown in Fig. 10(c), the fitting results for α_0 are $\alpha_{0,1} = 6056$, $\alpha_{0,0} = 1063$, and $\alpha_{0,-1} = -1.27$. It shows that the nonzero term $\alpha_{0,-1}$ gives diverging behavior and other all terms are same. Figure 10(d) shows that α_6 is linear function of δ_ν that passes through the origin and its value is $\alpha_{6,1} = -885$, $\alpha_{0,0} = 0$. It shows that it pass the origin, the zeroth order of α_6, $\alpha_{6,0}$, is zero and it approaches to zero when δ_ν becomes small.

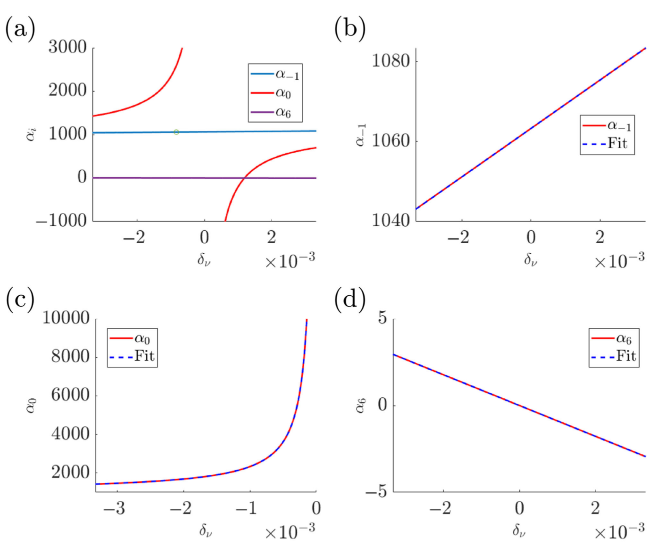

FIG. 10. Plot of coefficients and fittings. (a) Plot of α_{-1}, α_0 and α_6 vs δ_ν (b)–(d) precise plot of each coefficients and fitting results. Fitting was performed up to second order.

APPENDIX D: PROOF OF EQUIVALENCE BETWEEN TWO DETUNING PARAMETERS $\alpha_{x,x}$ AND α_0

In this section, we present a proof for the equivalence between two parameters

$$\alpha_0 = \frac{3}{2}\left(\sum_{n=-\infty}^{\infty} 3f_{3,0,n}g_{3,0,n} + \sum_{n=-\infty}^{\infty} f_{1,0,n}g_{1,0,n}\right), \tag{D1}$$

and

$$\alpha_{x,x} = -\frac{1}{64\pi}\int_0^L ds\, m(s)\beta_x^{\frac{3}{2}}(s) \times \int_s^{s+L} m(s')\beta_x^{\frac{3}{2}}(s')\left[\frac{\cos 3\Psi_x(s',s)}{\sin 3\pi\nu_x} + \frac{3\cos\Psi_x(s',s)}{\sin\pi\nu_x}\right]ds', \tag{D2}$$

where

$$\Psi_x(s',s) = \chi_x(s') - \chi_x(s) - \pi\nu_x. \tag{D3}$$

Equation (D1) is derived in the main article, Eq. (D2) is the well-known nonlinear detuning parameter. By applying the delta function approximation for the sextupole strength $m(s)$ into Eq. (D2), we show that the above equation is equivalent to Eq. (196) in [19]. To prove the equivalence, we separate integral form of the nonlinear detuning parameter $\alpha_{x,x}$ into two terms as follows:

$$\alpha_{x,x,3} = -\frac{1}{64\pi}\int_0^L ds\, m(s)\beta_x^{\frac{3}{2}}(s) \cdot \int_s^{s+L} m(s')\beta_x^{\frac{3}{2}}(s')\frac{\cos 3\Psi_x(s',s)}{\sin 3\pi\nu_x}ds', \tag{D4}$$

$$\alpha_{x,x,1} = -\frac{3}{64\pi}\int_0^L ds\, m(s)\beta_x^{\frac{3}{2}}(s) \cdot \int_s^{s+L} m(s')\beta_x^{\frac{3}{2}}(s')\frac{\cos \Psi_x(s',s)}{\sin \pi\nu_x}ds'. \tag{D5}$$

We express $\alpha_{x,x,3}$ as follows to facilitate further calculation,

$$\alpha_{x,x,3} = -\frac{1}{128\pi}\left(\int_0^L ds\, m(s)\beta_x^{\frac{3}{2}}(s)e^{-i3\chi_x(s)} \cdot \int_s^{s+L} m(s')\beta_x^{\frac{3}{2}}(s')e^{-i3\nu_x(\frac{s'-s}{R})}\frac{e^{i\Upsilon_x(s,s')}}{\sin 3\pi\nu_x}ds' + \int_0^L ds\; m(s)\beta_x^{\frac{3}{2}}(s)e^{i3\chi_x(s)} \cdot \int_s^{s+L} m(s')\beta_x^{\frac{3}{2}}(s')e^{i\cdot 3\nu_x(\frac{s'-s}{R})}\frac{e^{-i\Upsilon_x(s,s')}}{\sin 3\pi\nu_x}ds'\right), \tag{D6}$$

where

$$\Upsilon_x(s,s') \equiv 3\chi_x(s') - 3\pi\nu_x + 3\nu_x\left(\frac{s'-s}{R}\right). \tag{D7}$$

If we apply the following relation [20]

$$\sum_{n=-\infty}^{\infty}\frac{e^{i(n\theta+b)}}{n-3\nu_x} = -\frac{\pi}{\sin 3\pi\nu_x}e^{i[b+3\nu_x(\theta-\pi)]}, \tag{D8}$$

where $3\nu_x$ is not an integer, we can express Eq. (D6) as follows:

$$\alpha_{x,x,3} = \frac{1}{128\pi^2}\sum_{n=-\infty}^{\infty}\left\{\int_0^L ds\, m(s)\beta_x^{\frac{3}{2}}(s)e^{i(-3\chi_x(s)+\frac{3\nu_x s}{R}-\frac{ns}{R})}\int_s^{s+L} m(s')\beta_x^{\frac{3}{2}}(s')\frac{e^{i(\frac{ns'}{R}-\frac{3\nu_x s'}{R}+3\chi_x(s'))}}{n-3\nu_x}ds' + \int_0^L ds\, m(s)\beta_x^{\frac{3}{2}}(s)e^{i(3\chi_x(s)-\frac{3\nu_x s}{R}+\frac{ns}{R})}\times\int_s^{s+L} m(s')\beta_x^{\frac{3}{2}}(s')\frac{e^{-i(\frac{ns'}{R}-\frac{3\nu_x s'}{R}+3\chi_x(s'))}}{n-3\nu_x}ds'\right\}. \tag{D9}$$

The exponential function can be modified as follows due to the periodicity of the internal functions:

$$e^{i(n\frac{s'+L}{R}-3\nu_x(\frac{s'+L}{R})+3\chi_x(s'+L))} = e^{i(n\frac{s'}{R}-3\nu_x(\frac{s'}{R})+3\chi_x(s'))}. \tag{D10}$$

Using the relation in Eq. (D8), we can express Eq. (D6) by using Eqs. (A15) and (A16) as follows:

$$\begin{aligned}\alpha_{x,x,3} &= \frac{1}{128\pi^2}\sum_{n=-\infty}^{\infty}\left\{\int_0^L ds\, m(s)\beta_x^{\frac{3}{2}}(s)e^{i(-3\chi_x(s)+\frac{3\nu_x s}{R}-\frac{ns}{R})}\int_0^L m(s')\beta_x^{\frac{3}{2}}(s')\frac{e^{-i(-3\chi_x(s')+\frac{3\nu_x s'}{R}-\frac{ns'}{R})}}{n-3\nu_x}ds'\right.\\ &\quad\left.+\int_0^L ds\, m(s)\beta_x^{\frac{3}{2}}(s)e^{i(3\chi_x(s)-\frac{3\nu_x s}{R}+\frac{ns}{R})}\int_0^L m(s')\beta_x^{\frac{3}{2}}(s')\frac{e^{i(-3\chi_x(s')+\frac{3\nu_x s'}{R}-\frac{ns'}{R})}}{n-3\nu_x}ds'\right\}\\ &= \frac{3}{2}\sum_{n=\infty}^{\infty} 3g_{3,0,n}f_{3,0,n},\end{aligned} \tag{D11}$$

where $f_{3,0,n}$ is given in Eq. (34). By following a similar calculation process, we can also obtain the following relation:

$$\alpha_{x,x,1} = \frac{3}{2}\sum_{n=-\infty}^{\infty} g_{1,0,n}f_{1,0,n}. \tag{D12}$$

Thus, the nonlinear detuning parameter $\alpha_{x,x}$ is expressed by

$$\alpha_{x,x} = \alpha_{x,x,3} + \alpha_{x,x,1} = \frac{3}{2}\sum_{n=-\infty}^{\infty}(3g_{3,0,n}f_{3,0,n} + g_{1,0,n}f_{1,0,n}) = \alpha_0. \tag{D13}$$

As a result, we have demonstrated the equivalence of the two nonlinear detuning parameters given in Eqs. (D1) and (D2).

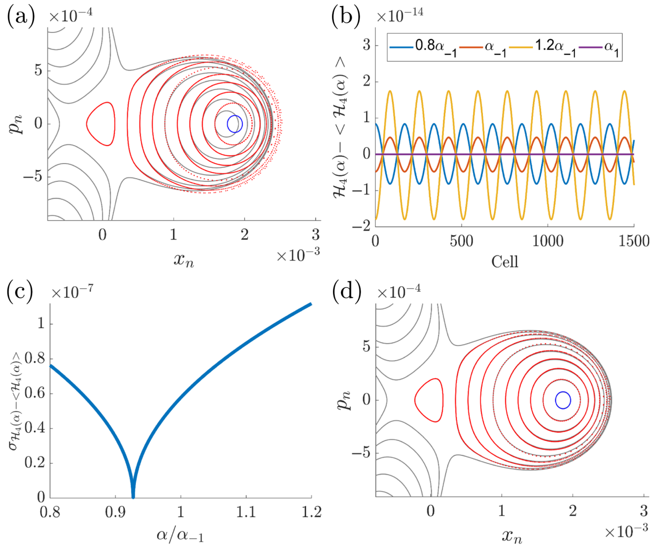

FIG. 11. α_1 calculating process (a) Tracking results of electron for 1500 cells and contour plot. The tracking was performed for every three cells to confine the results to a single island. The blue line represents the tracking results near the center of the islands. (b) Oscillation part of $\mathcal{H}_4$ for blue line of Fig. 11(a). It is defined by $(\mathcal{H}_4 - \langle\mathcal{H}_4\rangle)$ (c) We calculated the standard deviation of the oscillation part of $\mathcal{H}_4$ for the blue line in Fig. 11(a) and defined the value of α that minimizes the function $\sigma_{\mathcal{H}_4-\langle\mathcal{H}_4\rangle}$ as α_1. α_{-1} in x axis is 1058.1 and α_1 is 981.9. (d) Graph of tracking results and Hamiltonian contours in (a) and plot of Hamiltonian defined by using α_1.

APPENDIX E: DETERMINATION OF THE EMPIRICAL DETUNING PARAMETER α_1

This section describes the process used to determine the value of α_1 in this study. First, a tracking simulation was performed using an arbitrary value on the x axis as the initial point. This simulation was conducted over 1500 cells, using the lattice presented in Fig. 4 of main article. To ensure consistency, results were stored every three cells, ensuring all tracking simulation results were in the same island. The results are shown in Fig. 11(a).

Then, the point on the x axis closest to the fixed point of the island was identified from the tracking results. The blue line in Fig. 11(a) depicts the tracking result of the electron closest to the fixed point. Following this, the Hamiltonian was redefined as a function of α and the number of cells which electron passed and it is given by

$$\mathcal{H}_4 = \delta J + g_{3,0,l_{3\nu_x}} J^{\frac{3}{2}} \cos\left(3\psi + \xi_{3,0,l_{3\nu_x}}\right) + \frac{1}{2}\alpha J^2 \tag{E1}$$

The graph of the Hamiltonian's oscillation part for the electron closest to the fixed point at each α was obtained. This oscillation part was calculated by subtracting the mean value of the Hamiltonian with respect to its position from the Hamiltonian itself. The graph of the oscillation part of the Hamiltonian is shown in Fig. 11(b).

The value of α_1 was defined by computing the standard deviation of the oscillation part of the $\mathcal{H}_4$ for each α value and selecting the point where $\sigma_{\mathcal{H}_4-\langle\mathcal{H}_4\rangle}$ is minimized as α_1. This selection was made because the same particle has the same $\mathcal{H}_4$ values. Figure 11(c) shows the graph of the standard deviation of the oscillation part. The α value which has the minimum standard deviation corresponds to the value of α_1. Finally, α_1 was used to redraw the contour of the tracking results, and the Hamiltonian plot with α_1 is depicted in Fig. 11(d). This plot demonstrates that all electrons on the contour can be covered. Therefore, we can assume that α_1 is a reliable value.

APPENDIX F: CALCULATION OF THE RING AND RESONANCE ISLAND PARAMETERS AS A FUNCTION OF SEXTUPOLE STRENGTH IN A MIRROR-SYMMETRIC LATTICE

This section presents the derivation of the detuning parameters α_{-1} and α_0 as functions of sextupole strength, for a symmetric ring. Equation (D2) can be simplified by removing the s dependence of the integrand over the ds' integration range.

$$\alpha_0 = -\frac{1}{64\pi}\int_0^L\int_0^L m(s')m(s)\beta_x^{\frac{3}{2}}(s')\beta_x^{\frac{3}{2}}(s)\left(\frac{\cos 3\left(\pi\nu_x - |\chi_x(s') - \chi_x(s)|\right)}{\sin 3\pi\nu_x} + \frac{3\cos\left(\pi\nu_x - |\chi_x(s') - \chi_x(s)|\right)}{\sin \pi\nu_x}\right)ds'ds. \tag{F1}$$

To exploit the lattice symmetry, the integral range in the above equation can be shifted by $\frac{L}{2}$, resulting in the following expression:

$$\alpha_0 = -\frac{1}{64\pi}\int_{-\frac{L}{2}}^{\frac{L}{2}}\int_{-\frac{L}{2}}^{\frac{L}{2}} m_1(s')m_1(s)\beta_{x,1}^{\frac{3}{2}}(s')\beta_{x,1}^{\frac{3}{2}}(s)\left(\frac{\cos 3\left(\pi\nu_x - |\chi_x(s') - \chi_x(s)|\right)}{\sin 3\pi\nu_x} + \frac{3\cos\left(\pi\nu_x - |\chi_x(s') - \chi_x(s)|\right)}{\sin \pi\nu_x}\right)ds'ds. \tag{F2}$$

where $m_1(s) = m(s + \frac{L}{2})$ and $\beta_{x,1}(s) = \beta_x(s + \frac{L}{2})$. If the integral expression is rearranged such that the integral interval is limited to 0 to $\frac{L}{2}$, the resulting equation is as follows:

$$\alpha_0 = -\frac{2}{64\pi}\int_0^{\frac{L}{2}}\int_0^{\frac{L}{2}} m_1(s')m_1(s)\beta_{x,1}^{\frac{3}{2}}(s')\beta_{x,1}^{\frac{3}{2}}(s)[\{\cot 3\pi\nu_x\{\cos 3[\chi_x(s')-\chi_x(s)] + \cos 3[\chi_x(s')+\chi_x(s)]\} + \sin 3|\chi_x(s')-\chi_x(s)| + \sin 3(\chi_x(s')+\chi_x(s)]\} + 3\{\cot \pi\nu_x[\cos(\chi_x(s')-\chi_x(s)] + \cos[\chi_x(s')+\chi_x(s)]\} + \sin|\chi_x(s')-\chi_x(s)| + \sin[\chi_x(s')+\chi_x(s)]\}\})ds'ds, \tag{F3}$$

where s_i is the positive position of ith sextupole magnet, l_i is a length of ith sextupole magnet, S_i is a strength of sextupole magnet, and N is the number of sextupole magnets pairs. The index is arranged according to the distance from the origin and is restricted to sextupole magnets situated in the positive position due to their symmetrical distribution. Expressing the above equation as a quadratic function for the kth sextupole strength yields the following result:

$$\alpha_0(S_k) = a_{2,k}S_k^2 + 2a_{1,k}S_k + a_{0,k}, \tag{F4}$$

where $a_{2,k}$ is

$$a_{2,k} = -\frac{2}{64\pi}\int_{s_k}^{s_k+l_k}\int_{s_k}^{s_k+l_k}\beta_{x,1}^{\frac{3}{2}}(s')\beta_{x,1}^{\frac{3}{2}}(s)(2\cot 3\pi\delta_\nu \cos 3\chi_x(s)\cos 3\chi_x(s') + \sin 3|\chi_x(s')-\chi_x(s)| + \sin 3(\chi_x(s') + \chi_x(s)|) + 3\{2\cot\pi\nu_x\cos\chi_x(s')\cos\chi_x(s) + \sin|\chi_x(s')-\chi_x(s)| + \sin[\chi_x(s')+\chi_x(s)]\}\})ds'ds, \tag{F5}$$

$a_{1,k}$ is

$$a_{1,k} = -\frac{2}{64\pi}\sum_{i=1,i\neq k}^{N} S_i\int_{s_k}^{s_k+l_k}\int_{s_i}^{s_i+l_i}\beta_{x,1}^{\frac{3}{2}}(s')\beta_{x,1}^{\frac{3}{2}}(s)(2\cot 3\pi\delta_\nu\cos 3\chi_x(s)\cos 3\chi_x(s') + \sin 3|\chi_x(s')-\chi_x(s)| + \sin 3(|\chi_x(s')+\chi_x(s)|) + 3\{2\cot\pi\nu_x\cos\chi_x(s')\cos\chi_x(s) + \sin|\chi_x(s')-\chi_x(s)| + \sin[\chi_x(s')+\chi_x(s)]\}\})ds'ds, \tag{F6}$$

and $a_{0,k}$ is

$$a_{0,k} = -\frac{2}{64\pi}\sum_{i,j=1,i,j\neq k}^{N} S_iS_j\int_{s_j}^{s_j+l_j}\int_{s_i}^{s_i+l_i}\beta_{x,1}^{\frac{3}{2}}(s')\beta_{x,1}^{\frac{3}{2}}(s)(2\cot 3\pi\delta_\nu\cos 3\chi_x(s)\cos 3\chi_x(s') + \sin 3|\chi_x(s')-\chi_x(s)| + \sin 3(\chi_x(s')+\chi_x(s)|) + 3\{2\cot\pi\nu_x\cos\chi_x(s')\cos\chi_x(s) + \sin|\chi_x(s')-\chi_x(s)| + \sin[\chi_x(s')+\chi_x(s)]\}\})ds'ds. \tag{F7}$$

For a symmetric cell, the expression for $g_{3,0,l_{3\nu_x}}$ is given by

$$g_{3,0,l_{3\nu x}}\cos\xi_{3,0,l_{3\nu_x}} = \frac{\sqrt{2}}{12\pi}\sum_{i=1}^{N} S_i\int_{s_i}^{s_i+l_i}\beta_{x,1}^{\frac{3}{2}}(s)\cos\left(3\chi_x(s) - (3\nu_x - l_{3\nu_x})\frac{s}{R}\right)ds \equiv \sum_{i=1}^{N} S_i\mu_i. \tag{F8}$$

Hence, the expression for $g_{3,0,l_{3\nu_x}}^2$ is given by

$$\frac{3}{2\delta_\nu}g_{3,0,l_{3\nu x}}^2 = \frac{2}{96\delta_\nu\pi^2}\sum_{i,j=1}^{N} S_iS_j\int_{s_j}^{s_j+l_j}\int_{s_i}^{s_i+l_i}\beta_{x,1}^{\frac{3}{2}}(s')\beta_{x,1}^{\frac{3}{2}}(s)\cos\left(3\chi_x(s') - 3\delta_\nu\frac{s'}{R}\right)\cos\left(3\chi_x(s) - 3\delta_\nu\frac{s}{R}\right)ds'ds. \tag{F9}$$

Thus, the value of α_{-1} is obtained as follows:

$$\alpha_{-1} = -\frac{1}{32\pi}\sum_{i,j=1}^{N} S_i S_j \int_{s_j}^{s_j+l_j}\int_{s_i}^{s_i+l_i} \beta_{x,1}^{\frac{3}{2}}(s')\beta_{x,1}^{\frac{3}{2}}(s)\Bigg(2\cot 3\pi\nu_x \cos 3\chi_x(s)\cos 3\chi_x(s')$$
$$-\frac{2}{3\delta_\nu\pi}\cos\left(3\chi_x(s') - 3\delta_\nu\frac{s'}{R}\right)\cos\left(3\chi_x(s) - 3\delta_\nu\frac{s}{R}\right) + \sin 3|\chi_x(s') - \chi_x(s)|$$
$$+\sin 3[\chi_x(s') + \chi_x(s)] + 3\{2\cot\pi\nu_x\cos\chi_x(s)\cos\chi_x(s') + \sin|\chi_x(s') - \chi_x(s)| + \sin[\chi_x(s') + \chi_x(s)]\}\Bigg)ds'ds$$
$$\equiv \sum_{i,j=1}^{N} S_i S_j \mathcal{A}_{i,j} \tag{F10}$$

Expressing the above equation as a quadratic function for the kth sextupole strength yields the following result:

$$\alpha_{-1}(S_k) = b_{2,k}S_k^2 + 2b_{1,k}S_k + b_{0,k}, \tag{F11}$$

where $b_{1,k}$ is

$$b_{1,k} = -\frac{1}{32\pi}\sum_{i=1,i\neq k}^{N} S_i \int_{s_i}^{s_i+l_i}\int_{s_k}^{s_k+l_k} \beta_{x,1}^{\frac{3}{2}}(s')\beta_{x,1}^{\frac{3}{2}}(s)\Bigg(2\cot 3\pi\nu_x\cos 3\chi_x(s)\cos 3\chi_x(s')$$
$$-\frac{2}{3\delta_\nu\pi}\cos\left(3\chi_x(s') - 3\delta_\nu\frac{s'}{R}\right)\cos\left(3\chi_x(s) - 3\delta_\nu\frac{s}{R}\right) + \sin 3|\chi_x(s') - \chi_x(s)| + \sin 3[\chi_x(s') + \chi_x(s)]$$
$$+3\{2\cot\pi\nu_x\cos\chi_x(s)\cos\chi_x(s') + \sin|\chi_x(s') - \chi_x(s)| + \sin[\chi_x(s') + \chi_x(s)]\}\Bigg)ds'ds, \tag{F12}$$

$b_{0,k}$ is

$$b_{0,k} = -\frac{1}{32\pi}\sum_{i,j=1,i,j\neq k}^{N} S_i S_j \int_{s_i}^{s_i+l_i}\int_{s_j}^{s_j+l_j} \beta_{x,1}^{\frac{3}{2}}(s')\beta_{x,1}^{\frac{3}{2}}(s)\Bigg(2\cot 3\pi\nu_x\cos 3\chi_x(s)\cos 3\chi_x(s')$$
$$-\frac{2}{3\delta_\nu\pi}\cos\left(3\chi_x(s') - 3\delta_\nu\frac{s'}{R}\right)\cos\left(3\chi_x(s) - 3\delta_\nu\frac{s}{R}\right) + \sin 3|\chi_x(s') - \chi_x(s)| + \sin 3[\chi_x(s') + \chi_x(s)]$$
$$+3\{2\cot\pi\nu_x\cos\chi_x(s)\cos\chi_x(s') + \sin|\chi_x(s') - \chi_x(s)| + \sin[\chi_x(s') + \chi_x(s)]\}\Bigg)ds'ds, \tag{F13}$$

and $b_{2,k}$ is

$$b_{2,k} = -\frac{1}{32\pi}\int_{s_k}^{s_k+l_k}\int_{s_k}^{s_k+l_k} \beta_{x,1}^{\frac{3}{2}}(s')\beta_{x,1}^{\frac{3}{2}}(s)\Bigg(\frac{2}{3\pi\delta_\nu}\cos 3\chi_x(s)\cos 3\chi_x(s') - \frac{2}{3\pi\delta_\nu}\cos\left(3\chi_x(s) - 3\delta_\nu\frac{s}{R}\right)\cos\left(3\chi_x(s') - 3\delta_\nu\frac{s'}{R}\right)$$
$$-2\cos 3\chi_x(s)\cos\chi_x(s')\pi\delta_\nu + \sin 3|\chi_x(s') - \chi_x(s)| + \sin 3[\chi_x(s') + \chi_x(s)]$$
$$+3\{2\cot\pi\nu_x\cos\chi_x(s)\cos\chi_x(s') + \sin|\chi_x(s') - \chi_x(s)| + \sin[\chi_x(s') + \chi_x(s)]\}\Bigg)ds'ds. \tag{F14}$$

Taking the limit of $\delta_\nu \to 0$, we can use next relation,

$$\lim_{\delta_\nu\to 0}\left(\frac{\sin\left(\frac{3\delta_\nu}{2}\frac{s}{R}\right)}{3\pi\delta_\nu}\right) = \frac{s}{2\pi R}. \tag{F15}$$

Finally, $b_{2,k}$ is calculated as,

$$b_{2,k} = -\frac{1}{32\pi}\int_{s_k}^{s_k+l_k}\int_{s_k}^{s_k+l_k} \beta_{x,1}^{\frac{3}{2}}(s')\beta_{x,1}^{\frac{3}{2}}(s)\Bigg(-8\sin\left(3\chi_x(s') - \frac{3\delta_\nu}{2}\frac{s'}{R}\right)\cos\left(3\chi_x(s) - \frac{3\delta_\nu}{2}\frac{s}{R}\right)\cos\left(\frac{3\delta_\nu}{2}\frac{s}{R}\right)\frac{s'}{2\pi R}$$
$$-2\cos 3\chi_x(s)\cos 3\chi_x(s')\pi\delta_\nu + \sin 3|\chi_x(s') - \chi_x(s)| + \sin 3[\chi_x(s') + \chi_x(s)]$$
$$+3\{2\cot\pi\nu_x\cos\chi_x(s)\cos\chi_x(s') + \sin|\chi_x(s') - \chi_x(s)| + \sin[\chi_x(s') + \chi_x(s)]\}\Bigg)ds'ds. \tag{F16}$$

Due to the absence of δ_ν in the denominator, the coefficient $b_{2,k}$ remains finite for all values of δ_ν.

Horizontal and vertical chromaticities are given as follows:

$$\xi_{x,\mathrm{total}} = -\frac{1}{4\pi}\oint \beta_x(k - m\eta_x)ds, \tag{F17}$$

$$\xi_{y,\mathrm{total}} = \frac{1}{4\pi}\oint \beta_y(k - m\eta_x)ds, \tag{F18}$$

where k is the quadrupole distribution function, η_x is the horizontal dispersion function, β_y is the vertical betatron function, and the integral is performed over the inside of the cell. Chromaticity is represented as the sum of contributions from the sextupole and quadrupole components. Particularly, the terms $-\frac{1}{4\pi}\oint\beta_x k ds$ and $\frac{1}{4\pi}\oint\beta_y k ds$ arising from the quadrupole component are denoted as $\xi_{x,\mathrm{nat}}$ and $\xi_{y,\mathrm{nat}}$, respectively, and referred to as horizontal and vertical natural chromaticity. If the cell is mirror symmetric, Eqs. (F17) and (F18) can be arranged as linear functions with respect to the strengths of sextupoles as follows:

$$\xi_x \equiv \xi_{x,\mathrm{total}} - \xi_{x,\mathrm{nat}} = \sum_{i=1}^{N} S_i \frac{1}{2\pi}\int_{s_i}^{s_i+l_i} \beta_{x,1}\eta_{x,1} ds$$
$$\equiv \sum_{i=1}^{N} S_i \zeta_{x,i}, \tag{F19}$$

$$\xi_y \equiv \xi_{y,\mathrm{total}} - \xi_{y,\mathrm{nat}} = -\sum_{i=1}^{N} S_i \frac{1}{2\pi}\int_{s_i}^{s_i+l_i} \beta_{y,1}\eta_{x,1} ds$$
$$\equiv \sum_{i=1}^{N} S_i \zeta_{y,i}, \tag{F20}$$

where $\eta_{x,1} \equiv \eta_x(s + \frac{L}{2})$, $\beta_{y,1} \equiv \beta_y(s + \frac{L}{2})$.

[1] R. Cappi and M. Giovannozzi, Phys. Rev. Lett. **88**, 104801 (2002).
[2] M. Giovannozzi, L. Huang, A. Huschauer, and A. Franchi, Eur. Phys. J. Plus **136**, 1189 (2021).
[3] M. Giovannozzi and J. Morel, Phys. Rev. ST Accel. Beams **10**, 034001 (2007).
[4] A. Franchi, S. Gilardoni, and M. Giovannozzi, Phys. Rev. ST Accel. Beams **12**, 014001 (2009).
[5] P. Goslawski, F. Andreas, F. Armborst, T. Atkinson, J. Feikes, A. Jankowiak, J. Li, T. Mertens, M. Ries, A. Schälicke *et al.*, in *Proceedings of 10th International Particle Accelerator Conference, IPAC-2019, Melbourne, Australia* (JACoW, Geneva, Switzerland, 2019), pp. 3419–3422.
[6] D. Robin, C. Steier, J. Safranek, and W. Decking, in *Proceedings of the 7th European Particle Accelerator Conference, Vienna, Austria, 2000* (JACoW, Geneva, Switzerland, 2000), pp. 136–140.
[7] J. Kim, J. A. Safranek, and K. Tian, in *Proceedings of 13th International Particle Accelerator Conference, IPAC-2022, Bangkok, Thailand* (JACoW, Geneva, Switzerland, 2022), pp. 203–206.
[8] K. Holldack, C. Schüßler-Langeheine, N. Pontius, T. Kachel, P. Baumgärtel, Y. W. Windsor, D. Zahn, P. Goslawski, M. Koopmans, and M. Ries, Sci. Rep. **12**, 14876 (2022).
[9] K. Holldack, C. Schüssler-Langeheine, P. Goslawski, N. Pontius, T. Kachel, F. Armborst, M. Ries, A. Schälicke, M. Scheer, W. Frentrup *et al.*, Commun. Phys. **3**, 61 (2020).
[10] D. K. Olsson and A. Andersson, Nucl. Instrum. Methods Phys. Res., Sect. A **1017**, 165802 (2021).
[11] J. G. Hwang, G. Schiwietz, M. Abo-Bakr, T. Atkinson, M. Ries, P. Goslawski, G. Klemz, R. Muller, A. Schulicke, and A. Jankowiak, Sci. Rep. **10**, 10093 (2020).
[12] T. Arion, W. Eberhardt, J. Feikes, A. Gottwald, P. Goslawski, A. Hoehl, H. Kaser, M. Kolbe, J. Li, C. Lupulescu, M. Richter, M. Ries, F. Roth, M. Ruprecht, T. Tydecks, and G. Wustefeld, Rev. Sci. Instrum. **89**, 103114 (2018).
[13] M. A. Jebramcik, S. Khan, and W. Helml, Sci. Rep. **12**, 18383 (2022).
[14] S. Ferraz-Mello, *Canonical Perturbation Theories. Degenerate Systems and Resonance*, 1st ed., Astrophysics and Space Science Library Vol. 345 (Springer, New York, NY, 2007).
[15] G. Guignard, A general treatment of resonances in accelerators, CERN, Technical Report No. CERN 78-11, 1978.
[16] H. Wiedemann, *Particle Accelerator Physics*, 3rd ed. (Springer, Berlin, Heidelberg, 2007).
[17] K. Soutome and H. Tanaka, Phys. Rev. Accel. Beams **20**, 064001 (2017).
[18] M. Takao, Phys. Rev. E **72**, 046502 (2005).
[19] S. Y. Lee, *Accelerator Physics*, 4th ed. (World Scientific Co. Pte. Ltd., Singapore, 2019).
[20] N. Merminga and K. Ng, Two-fifth resonance islands generated by sextupoles, FERMILAB, Technical Report No. FN-506, 1992.
[21] A. Bazzani, G. Servizi, E. Todesco, and G. Turchetti, A normal form approach to the theory of nonlinear betatronic motion, *CERN Yellow Reports: Monographs* (CERN, Geneva, 1994).
[22] S. T. Wang, V. Khachatryan, and P. Nishikawa, Phys. Rev. Accel. Beams **26**, 104001 (2023).
[23] R. D. Ruth, AIP Conf. Proc. **153**, 150 (1987).
[24] S. Shin, S. Kwon, D. Kim, D. Kim, M. Kim, S. Kim, S. Kim, J. Kim, C. Kim, B. Park *et al.*, J. Instrum. **8**, P01019 (2013).
[25] E. Jaeschke, D. Kramer, B. Kuske, P. Kuske, M. Scheer, E. Weihreter, and G. Wustefeld, in *Proceedings of International Conference on Particle Accelerators* (IEEE, New York, 1993), Vol. 2, pp. 1474–1476.